This is the peer-reviewed, final accepted version for American Mineralogist, published by the Mineralogical Society of America.
The published version is subject to change. Cite as Authors (Year) Title. American Mineralogist, in press.
DOI: https://doi.org/10.2138/am-2022-8738. http://www.minsocam.org/

Revision 1

CURIES: Compendium of Uranium Raman and Infrared Experimental Spectra

Tyler L. Spano[1], Travis A. Olds[2], Marshall McDonnell[3], Robert Smith[3], Jennifer L. Niedziela[1], Andrew Miskowiec[1], Roger Kapsimalis[1], Ashley E. Shields[1]

[1]*Nuclear Nonproliferation Division, Oak Ridge National Laboratory, 1 Bethel Valley Rd., Oak Ridge, TN 37830*

[2]*Carnegie Museum of Natural History, 4400 Forbes Ave., Pittsburgh, PA 15213*

[3]*Computer Science and Mathematics Division, Oak Ridge National Laboratory, 1 Bethel Valley Rd., Oak Ridge, TN 37830*

Abstract

Identification of radioactive materials is a critical goal of resource exploration, basic actinide science, and nuclear forensics, and we provide here new insights towards rapid, nondestructive analysis of uranium-containing minerals and technogenic phases. Raman and infrared spectroscopic methods are powerful indicators of solid-phase U(VI) coordination chemistry. In addition, U(VI) minerals exhibit high chemical and structural diversity as artifacts of geochemical processes leading to ore formation. Spectral signals of axial UO_2^{2+} ($U–O_{yl}$) bond lengths and the influences of additional oxyanions on these values are well documented for uranium oxide and oxysalt minerals and technogenic phases. Additional insight regarding the underlying crystallographic structure and chemical composition of uranium materials can be extracted through a survey of all available Raman spectroscopic data for these phases. To this end, we have developed the Compendium of Uranium Raman and Infrared Experimental Spectra (CURIES). CURIES was compiled via thorough review of literature and databases and for mineral species that lack measured and recorded spectra, data were obtained either from museum and academic collections or by direct syntheses. Characteristic Raman spectroscopic features for subgroups of uranyl minerals within CURIES were elucidated using multivariate statistical

analyses. In addition, average spectra for groups of uranyl minerals were determined, providing insight into common spectroscopic characteristics that are indicative of the structural origins from which they arise. As of publication, 275 mineral species and technogenic phases have been entered in CURIES, and of these, 83 phases have published spectra that have been included in the CURIES database. Data collection is ongoing, and we have triaged missing data sets to assess CURIES for completion and to identify mineral groups that lack representation and should therefore be prioritized for data acquisition and inclusion in the database.

Keywords: U(VI) minerals, uranyl minerals, Raman PLSR, Raman PCA, mineral spectroscopy

Introduction

A long-standing question in mineralogy is how to relate observed spectroscopic features more closely to the underlying crystal structure from which they originate. In addition, accurate identification of uranium-bearing compounds remains a significant challenge in the fields of nuclear forensics (Lin et al., 2013; Palacios and Taylor, 2000; Pointurier and Marie, 2010), environmental remediation (Amme et al., 2002; Christensen et al., 2004; Faulques et al., 2015b), and resource exploration (Beiswenger et al., 2018; Stefaniak et al., 2008). Although vibrational spectroscopic signatures are well documented as powerful indicators of physiochemical properties of nuclear materials relevant to the fuel cycle (Bonales et al., 2016b; Kirkegaard et al., 2020; Lv et al., 2016; Schwerdt et al., 2018; Spano et al., 2020b; Sweet et al., 2013), and are often reported in investigations of new mineral species, existing spectroscopic analysis platforms (Laetsch and Downs, 2006) rely on pattern matching between the collected spectrum and a database. Unfortunately, an exhaustive library of high-fidelity experimental spectroscopic data is not currently available for nuclear fuel cycle materials, nor have all available optical vibrational spectra for uranium minerals been collated. Because many naturally occurring uranium minerals

possess structural and chemical similarities to technogenic fuel cycle materials, compilation of these data into a compendium represents a transformative capability towards rapid and nondestructive identification of both uranium minerals and fuel cycle materials (Forsyth et al., 1986; Guo et al., 2014; Kirkegaard et al., 2020; Kirkegaard et al., 2019; McNamara et al., 2002; Plášil, 2014; Spano et al., 2020a).

Low symmetry crystals and amorphous systems are commonly observed in nuclear fuel cycle materials. Similarly, poorly crystalline, or admixed mineral species are often encountered. These scenarios can lead to broadening of spectroscopic information such that simple pattern matching cannot provide additional information about the sample. Nevertheless, spectral information is retained in these amorphous, admixed, and/ or poorly crystalline systems that can be indicative of specific structural subunits (i.e., chemical coordination environment, additional oxyanion species)(Spano et al., 2020a). By relating the local chemical environment probed by Raman and/or infrared (IR) to a specific structural subunit or chemical environment (Čejka, 1999; Lu et al., 2018), one can ascertain new information relating amorphous and other nonideal samples to a specific chemical, geologic, or environmental process that led to its formation.

Strong correlations between the location of the symmetric uranyl stretching vibrational mode in Raman and IR spectra and the U-O_{yl} bond length are well documented (Bartlett and Cooney, 1989; Glebov, 1982; Jones, 1958; Lu et al., 2018). Similarly, an extensive review of spectroscopic features in the IR spectra of uranyl minerals was conducted in 1999 (Čejka, 1999). Recent work has also explored the relationship between coordination environment, oxyanion speciation, and the resulting range of uranyl bond lengths in U(VI) phases (Lu et al., 2018). However, no large-scale account of salient features (beyond characteristic U-O_{yl} vibrational modes) common to groups of uranyl minerals based on oxyanion chemistry has been reported.

Explicit assignment of the Raman and IR-active phonon modes in materials is possible using ab initio calculations (e.g., density functional theory, DFT). However, DFT calculations of the lattice dynamics can quickly become computationally expensive for mineral phases because of missing or incomplete structural information and complicated crystal systems with large unit cells and low symmetry. Additionally, uranyl minerals rarely adopt an ideal end-member composition and often contain significant substitutions of interlayer cations, as well as variable hydration states for some species. Owing to the large number of secondary uranium minerals, it is impractical to attempt to use ab initio methods to understand the structural origin of spectral features on a sample-by-sample basis, however, by utilizing a large basis set of experimental spectroscopic data, we demonstrate the efficient ability to realize salient spectroscopic features that are common to groups of uranyl minerals based on oxyanion species.

While extensive reviews of U(VI) crystal structures are available (Burns, 2005; Burns et al., 1997; Lussier et al., 2016), as are general spectroscopic databases (Baldridge et al., 2009; Lafuente B, 2015), no single database exists to house vibrational spectroscopic, crystallographic, and related metadata for secondary uranium minerals exclusively. To this end, we have conducted an exhaustive literature review to catalog all presently known secondary uranium mineral species, and a currently existing database (Lafuente B, 2015). to compile all available Raman and IR spectroscopic data and all available crystallographic and associated metadata to construct CURIES, a compendium of uranium Raman and IR experimental spectra.

Using the compendium, we now have a robust baseline to generate new spectroscopic insights. As a first demonstration of potential applications for CURIES, we calculated the average Raman spectra for groups of uranyl minerals based on oxyanion chemistry, used multivariate statistical analysis including principal component analysis (PCA) and partial least

96 squares regression (PLSR), and combined these methods to gain insight into the structural
97 origins of common features found in Raman spectra of secondary U minerals (Corcoran et al.,
98 2019; Ho et al., 2015). As an alternative to large-scale computational investigations, our goal is
99 to provide the community with an up-to-date summary of optical vibrational spectroscopic data
100 for uranyl minerals that can be employed for pattern matching, phase identification, and to gain
101 insight into the underlying chemistry of new phases via rapid, nondestructive spectroscopic
102 analyses. Moving forward, we seek to expand the available data in CURIES. Therefore, we
103 present statistics regarding the percentage of spectra for groups of uranyl minerals that have been
104 included in the compendium as a guide for future synthesis work, collaboration with museum
105 partners, and, ideally, readers of this work.

106 **Methods**

107 Supergene uranium mineral speciation was examined first using extensive reviews by
108 Burns(2005), Lussier et al.(2016), Plášil (2014), and the mineralogical database Mindat (Ralph
109 and Chau, 2014). Mindat, which sources data from the International Mineralogical Association
110 (IMA) Commission on New Minerals, Nomenclature and Classification provides the most up-to-
111 date information regarding reported mineral species. Using Mindat's "search by chemistry"
112 feature, groups of secondary uranium minerals were retrieved based on oxyanion species. For
113 example, a search on "contains U and P" returned all reported uranyl phosphate species. We note
114 that in addition to mineral species recognized by the IMA, unnamed minerals and discredited
115 species are also returned on these searches, and these have not been included in our analyses.

116 Mindat results were tabulated into summary spreadsheets for each group of uranyl
117 minerals. Crystal chemical and structural information, including formula, space group, formula
118 units per unit cell, and density were also included when available from Mindat and were verified,

when possible, by examination of crystal structure data. All available literature references for each uranium mineral in Mindat were examined and compiled, though not all literature references are included here. For brevity, references are prioritized to those providing a structure and/or spectra of a given species.

Once lists of U minerals based on oxyanion group were tabulated, we used the RRUFF database to find existing Raman and IR spectra for each species. Data were exported as they appear in the database, and, in some cases, have been listed as candidates for recollection of data where spectral resolution or data quality is poor. For each spectral file extracted from RRUFF (Lafuente B, 2015), a unique filename was created within CURIES. The spectral data are then associated with metadata pertaining to the acquisition parameters, including the excitation wavelength and instrument used to collect Raman data, and laser power. Additional methods of phase identification (e.g., X-ray diffraction, elemental analysis via scanning electron microscopy-energy dispersive spectroscopy) were noted in the metadata. Associated mineral species that might contribute to a given spectrum (i.e., as a minor phase or contaminant) were also included as metadata. For spectra not available within the RRUFF database, supplementary information of literature references for each species were consulted, and, when possible, these data sets were extracted from the publication and included in CURIES (Supporting Information).

After the literature review was completed, additional species that were known to exist but had no associated spectral data were triaged for spectral data acquisition. Mineral and synthetic analogue data collected by us were also included in the initial CURIES database. For these entries, additional information including synthesis methods and details of storage, or aging of samples, is included where available.

In addition to optical vibrational spectra, crystallographic information were compiled where available and associated to the relevant CURIES entries. Crystallographic information files (CIFs) were obtained using the American Mineralogist Crystal Structure Database, Inorganic Crystal Structure Database, and the Crystallography Open Database (Supporting Information). When multiple CIF files were available for a given mineral, the most recent CIF, or the one with the highest quality data were chosen for metadata extraction. The crystal structure of the mineral schoepite ($(UO_2)_8O_2(OH)_{12} \cdot 12H_2O$), for example, was described in 1996 by Finch et al. (Finch et al., 1996) and was recently reexamined by Plášil(2018). The recent work discovered additional complexity, with a higher symmetry space group (*Pbca* vs. $P2_1ca$) indicated by their X-ray crystallographic results. Thus, the updated structure was chosen for inclusion in CURIES. Similarly, two crystal structures are reported for boltwoodite ($(K,Na)(UO_2)(SiO_3OH)\cdot 1.5H_2O$). The first, published in 1981, located U, K, and Si sites, six O atoms, and one water molecule (Stohl and Smith, 1981). The second structure determination for boltwoodite included partial Na substitution for K and identified an additional water molecule (Burns, 1998a). The latter was thus chosen for incorporation into the CURIES database.

Each CIF file included in CURIES was examined manually to ensure structural models are reasonable and to determine U coordination environments and bond lengths. Particular attention was paid to U coordination centers. For each CIF file, the number of independent sites and type of U coordination polyhedron was noted (square, pentagonal, and/or hexagonal bipyramidal), along with average UO_2^{2+} (uranyl, U-O_{yl}) and equatorial (U-O_{eq}) bond lengths (Burns et al., 1997). From this manual examination of CIF files combined with review of associated literature, several structures were identified as requiring additional analysis or reformatting as indicated by incomplete or incorrect atom placement or file formatting issues, for

example. Further X-ray diffraction experiments, symmetry analyses (e.g. via PLATON software package (Spek, 2009)), computational structure optimization via DFT, or a combination of these methods may prove beneficial towards a more complete understanding of U mineral species. While reexamination of these species is beyond the scope of this work, bijvoetite-Y ($Y_8(UO_2)_{16}(CO_3)_{16}O_8(OH)_8 \cdot 39H_2O$ (Li et al., 2000) and carnotite ($K_2(UO_2)_2(VO_4)_2 \cdot 3H_2O$) (Barton Jr, 1958)were some of the structures identified in this way. The CIF file available for bijvoetite-Y possesses unreasonably short metal-oxygen bond distances (e.g. ~1.25 Å for U-O). The carnotite CIF is missing several O atoms, for instance, the VO_4 square pyramidal coordination environments characteristic of uranyl sorovanadates are not fully coordinated and appear as tetrahedra.

Although IR spectra are included in CURIES, we have chosen to focus our analysis discussion on the compiled Raman spectra as a first demonstration. Individual Raman spectra were separated for analysis based on the excitation wavelength used for data collection (typically 785/780 or 532 nm) and were imported to OriginPro2021 (OriginLab Corporation, Northampton, Massachusetts, USA) for bulk processing based on oxyanion chemistry. First, we applied linear interpolation to raw data (Figure 1a) to ensure consistent wavenumber spacing (0.875 cm^{-1}) and data ranges (250–2000 cm^{-1}, Figure 1b) across all spectra. Next, spectral intensity was normalized to total counts (intensity at each datapoint divided by the sum of total intensity) to ensure equal weighting during multivariate statistical analyses (Figure 1c). Although we recognize that this normalization scheme is not ideal, nor is it the most rigorous method by which to conduct data processing, this is the most consistent and rapid way to treat the numerous data sets of varying origin that are included in CURIES.

This is the peer-reviewed, final accepted version for American Mineralogist, published by the Mineralogical Society of America.
The published version is subject to change. Cite as Authors (Year) Title. American Mineralogist, in press.
DOI: https://doi.org/10.2138/am-2022-8738. http://www.minsocam.org/

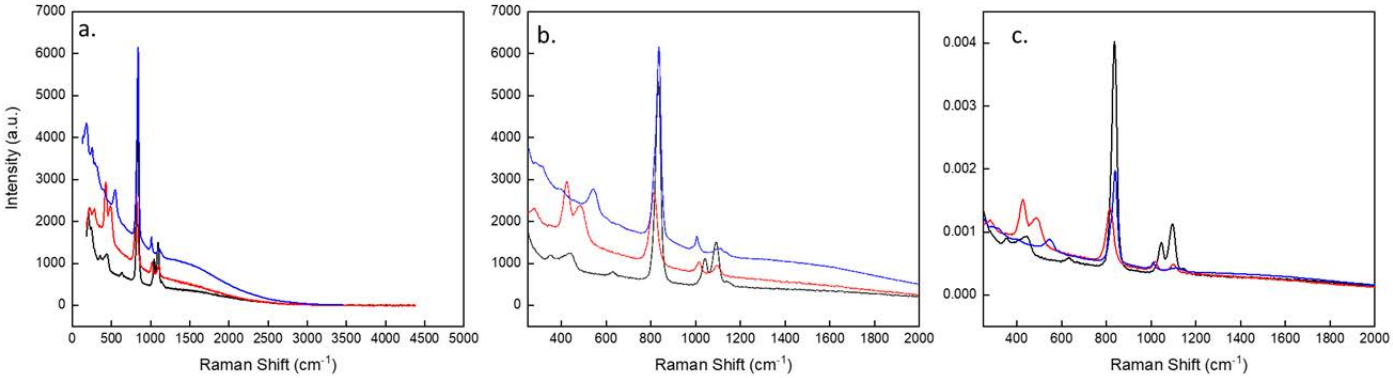

186

187 *Figure 1. Spectra of uranyl sulfate minerals johannite, marecottite, and uranopilite (a) as downloaded*
188 *from the RRUFF database, (b) following linear interpolation, and (c) following intensity normalization.*

189 To look for consistent spectral features, we calculated the average spectra for each group
190 of uranyl minerals based on oxyanion chemistry (e.g., uranyl phosphates, uranyl carbonates).
191 Following the normalization schemes described previously, we computed the average spectra for
192 each mineral group (Figure 2) by summing the interpolated, normalized intensities and
193 subsequently dividing by the number of mineral species included in each oxyanion subgroup. For
194 example, spectra for 10 uranyl hydroxide species are included in in the average spectrum for this
195 mineral group. The normalized intensities at each wavenumber were summed and then divided
196 by 10 to determine the average uranyl hydroxide spectrum.

This is the peer-reviewed, final accepted version for American Mineralogist, published by the Mineralogical Society of America.
The published version is subject to change. Cite as Authors (Year) Title. American Mineralogist, in press.
DOI: https://doi.org/10.2138/am-2022-8738. http://www.minsocam.org/

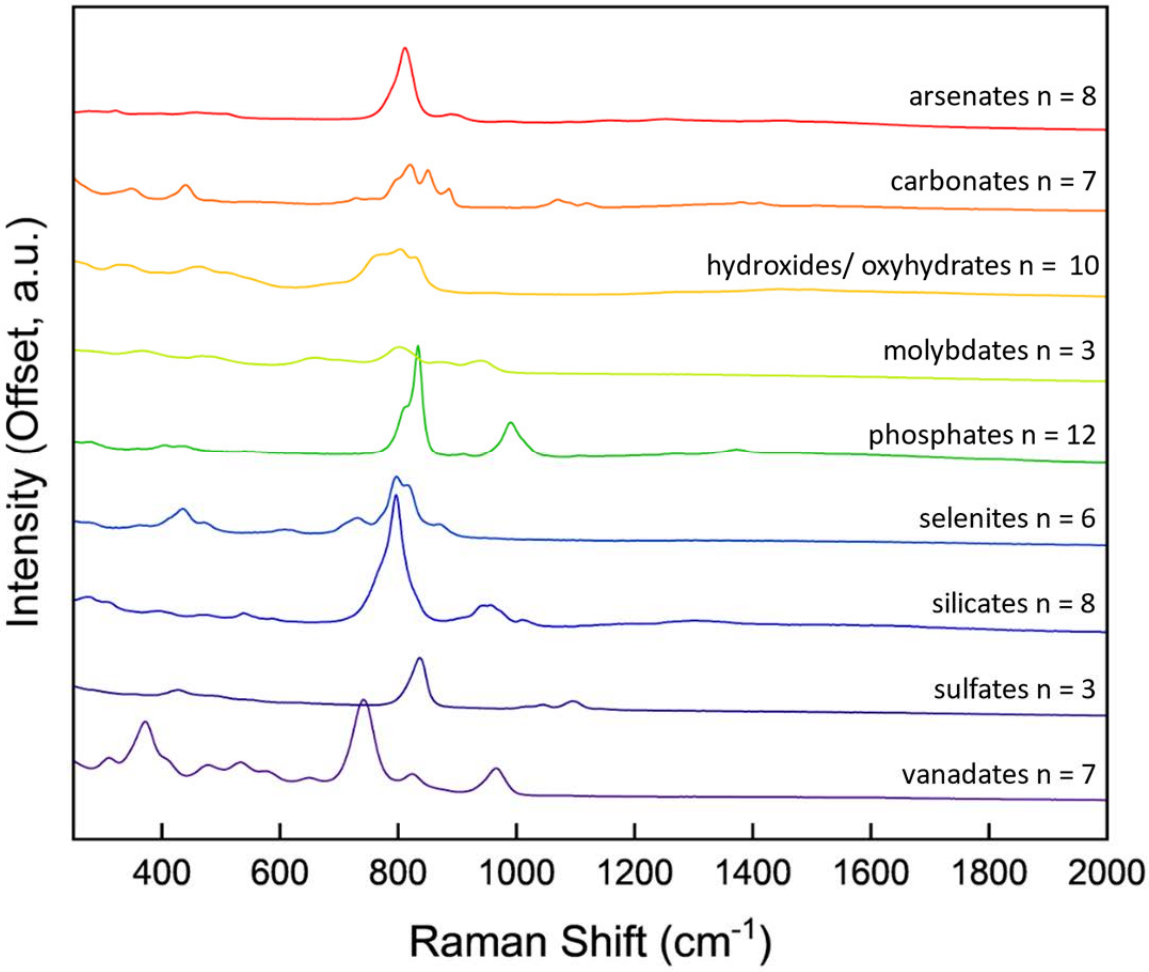

Figure 2. Average spectra (offset) for groups of uranyl minerals based on oxyanion chemistry. The number of mineral species included in the average are indicated.

Some mineral species within CURIES have several associated data sets. Although all available data sets for each mineral species entered in CURIES are included in our database, to prevent oversampling of species with multiple data sets and therefore biasing the average spectra for groups of uranyl minerals, only one spectrum for each mineral species is included in the average spectra seen in Figure 2. For example, literature review yielded three separate Raman data sets for the uranyl hydroxide mineral curite, $Pb_3(H_2O)_2[(UO_2)_4O_4(OH)_3]_2$. Before including

206 spectra for curite in the uranyl hydroxide average spectrum (technically, this is the average
207 spectrum of uranyl oxyhydrates, hydroxides and uranyl oxy-hydroxy-hydrates, but we use the
208 general term "hydroxides" for conciseness throughout), the three normalized data sets for this
209 species were summed and then divided by 3 to determine the average curite spectrum. Similarly,
210 polyanionic uranyl mineral species, schröckingerite, $NaCa_3(UO_2)(CO_3)_3(SO_4)F\cdot 10H_2O$, for
211 example, were excluded from both the uranyl carbonate and uranyl sulfate spectra with which
212 this mineral could be grouped.

213 Average spectra calculated for each group of uranyl minerals were then fit to Voigt
214 profiles using the Fityk software package (Wojdyr, 2010) via a Levenberg Marquardt nonlinear
215 least squares method. Fitting these average spectra enabled identification of characteristic
216 spectral features associated with underlying crystal-chemical attributes unique to these groups of
217 uranyl minerals.

218 Principal component analyses were done in OriginPro2021 using normalized data.
219 Raman shift (cm^{-1}) was input as observations, whereas normalized intensity at each wavenumber
220 for each mineral spectra were input as variables. Initially, two principal components were
221 identified, and based on Scree plots, additional components were added to account for maximum
222 variability amongst spectra. Ten principal components were identified in this way and account
223 for 92.91% of variability amongst spectra.

224 To examine similarities in spectra that may not be immediately obvious from our average
225 spectra computed for each mineral group, principal component (PC) spectra, generated from
226 PCA, were compared with average spectra to determine contributions that might result from
227 more subtle, underlying structural features. Interpretation was done by creating overlays of PC
228 spectra and average spectra for each of the mineral groups, and, more quantitatively, through

PLSR of PC spectra to determine the likelihood that spectra for a given oxyanion group is contributing to a PC spectrum.

Results and Discussion

Average Spectra for Mineral Groups by Oxyanion Chemistry

Towards our goal of identifying additional spectroscopic features beyond the characteristic uranyl vibrational mode present in the spectra of U(VI) mineral species (Lu et al., 2018), we have calculated the average Raman spectrum for groups of uranyl minerals based on oxyanion chemistry. This analysis has elucidated prominent spectral features that are associated with these mineral groups (Table 1) (Driscoll et al., 2014). As described in the previous section, average spectra were fit to Voigt profiles, and deconvolution was performed to assist in our assignment of observed spectral features to structural attributes from which they may originate. Literature precedent for this type of analysis exists as a similar approach was taken towards identifying unique indicators of trace element chemistry as a function of geologic deposit type for uranium ores (Spano et al., 2017b). For some groups of uranyl minerals, we acknowledge that lack of available spectra could lead to an incomplete understanding of characteristic spectral features for this group. To this end we have tabulated the number of mineral species included in CURIES and the number of spectra associated with each mineral group in Table 2. In addition to providing insight into high-priority targets for inclusion in CURIES, and, hopefully, illustrating to readers of this work where their spectral contributions can support our effort, Table 2 also allows us to approach our interpretation of average mineral spectra with candor.

This is the peer-reviewed, final accepted version for American Mineralogist, published by the Mineralogical Society of America.
The published version is subject to change. Cite as Authors (Year) Title. American Mineralogist, in press.
DOI: https://doi.org/10.2138/am-2022-8738. http://www.minsocam.org/

249 *Table 1. Raman assignments for average spectra*

Feature (cm^{-1})	Uranyl Mineral Group	Assignment	Reference
811	arsenates	$\nu_1UO_2^{2+}$, $\nu_1AsO_4^{3-}$, $\nu_3AsO_4^{3-}$	Plášil 2010
895	arsenates	$\nu_1AsO_4^{3-}$, $\nu_3UO_2^{2+}$*	Plášil 2010, Driscoll et al., 2014
450-525	arsenates	$\nu_2AsO_4^{3-}$,$\nu_4AsO_4^{3-}$	Plášil 2010
320-380	arsenates	$\nu_2AsO_4^{3-}$	Plášil 2010
1375-1400	carbonates	$\nu_3CO_3^{2-}$	Bonales et al., 2016, Frost et al., 2009, Driscoll et al., 2014
1025-1150	carbonates	$\nu_1CO_3^{2-}$	Bonales et al., 2016, Driscoll et al., 2014
824-851	carbonates	$\nu_1UO_2^{2+}$	Bonales et al., 2016
760	carbonates	δCO_3^{2-} out of plane deformation	Bonales et al., 2016, Driscoll et al., 2014
728	carbonates	δCO_3^{2-} in plane bending	Bonales et al., 2016, Driscoll et al., 2014
1440-1500	hydroxides/ oxyhydrates	δ-U-OH bending, ν_1 and $\nu_2UO_2^{2+}$ combination bands and overtones	Frost et al., 2007, Colmenero et al., 2019
754-832	hydroxides/ oxyhydrates	$\nu_1UO_2^{2+}$	Frost et al., 2007
~800	molybdates	$\nu_1UO_2^{2+}$	Frost et al., 2008
368-470	molybdates	$\nu_1MoO_4^{2-}$	Frost et al., 2008
990-1021	phosphates	$\nu_1PO_4^{3-}$, $\nu_3PO_4^{3-}$	Frost et al., 2004, Driscoll et al., 2014
740-870	phosphates	$\nu_1UO_2^{2+}$	Frost et al., 2004, Driscoll et al., 2014
560-660	phosphates	$\nu_4PO_4^{3-}$	Driscoll et al., 2014
370-480	phosphates	$\nu_2PO_4^{3-}$,	Driscoll et al., 2014
790-855	selenites	$\nu_1SeO_3^{2-}$	Frost et al., 2006
680-775	selenites	$\nu_3SeO_3^{2-}$	Frost et al., 2006
~460	selenites	$\nu_2SeO_3^{2-}$	Frost et al., 2006
387-418	selenites	$\nu_4SeO_3^{2-}$	Frost et al., 2006
925-1025	silicates	νSiO_4^{4-}	Frost et al., 2005
700-850	silicates	$\nu_1UO_2^{2+}$	Frost et al., 2005
450-650	silicates	δ, ν_4 SiO_4^{4-}	Frost et al., 2005
1000-1179	sulfates	$\nu_1SO_4^{3-}$, $\nu_3SO_4^{3-}$	Frost et al., 2005, Makreski et al., 2005
778-880	sulfates	$\nu_1UO_2^{2+}$	Frost et al., 2005, Makreski et al., 2005
625-670	sulfates	$\nu_4SO_4^{3-}$	Frost et al., 2005, Makreski et al., 2005
420-450	sulfates	$\nu_2SO_4^{3-}$	Frost et al., 2005, Makreski et al., 2005
950-975	vanadates	ν_1VO_3	Frost et al., 2005
~860	vanadates	$\nu_1UO_2^{2}$ǂ	Frost et al., 2005
~750	vanadates	ν_2VO_5, ν_3VO_5	Frost et al., 2005
450-575	vanadates	U-O equatorial modes	Frost et al., 2005
~370	Vanadates	V_2O_2 bending	Frost et al., 2005

* $\nu_3UO_2^{2+}$ are unlikely without significant structural disorder, ν_3 is Raman silent based upon selection rules.
ǂ Less intense than V-O modes at 750 cm^{-1}

250

251 *Table 2. CURIES status and completion*

Mineral Group	Number of species included in CURIES	Number of spectra included in CURIES	% Completion
Arsenates	38	7	18
Carbonates	36	11	30
Hydroxides	37	14	37
Phosphates	51	13	25
Silicates	23	10	43
Sulfates	55	6	10
Vanadates	14	9	64
Other (Selenites, molybdates, mixed chemistry phases)	18	9	50
Overall	275	77	28

252

253 *Uranyl Arsenates*

The spectra of arsenuranospathite ($Al(UO_2)_2(AsO_4)_2F{\cdot}20H_2O$) (Bo et al., 2015), chistyakovaite ($Al(UO_2)_2(AsO_4)_2(F,OH) \cdot 6.5H_2O$) (Chukanov et al., 2006), heinrichite ($Ba(UO_2)_2(AsO_4)_2{\cdot}10H_2O$) (Geipel et al., 2000; Gross et al., 1958), metaheinrichite ($Ba(UO_2)_2(AsO_4)_2{\cdot}8H_2O$) (Geipel et al., 2000; Gross et al., 1958), metarauchite ($Ni(UO_2)_2(AsO_4)_2{\cdot}8H_2O$) (Plášil, 2010), metazeunerite ($Cu(UO_2)_2(AsO_4)_2 \cdot 8H_2O$) (Locock and Burns, 2003), uramarsite ($(NH_4,H_3O)_2(UO_2)_2(AsO_4,PO_4)_2{\cdot}6H_2O$) (Chukanov, 2013; Sidorenko et al., 2007), and walpurgite ($(BiO)_4(UO_2)(AsO_4)_2{\cdot}2H_2O$)(Frost et al., 2006f; Mereiter, 1982b) make up the calculated average uranyl arsenate spectra. Less complexity is observed in the average spectra calculated for uranyl arsenates relative to uranyl carbonates and hydroxides/oxyhydrates, which are discussed later. A high-intensity vibrational mode is in the uranyl region, centered at 811 cm^{-1}, and is composed of contributions from three peaks as indicated by spectral deconvolution. In this region, both uranyl and arsenate vibrations contribute to observed intensity (Plášil, 2010). The other salient feature of the average uranyl arsenate spectra is a mode centered at 895 cm^{-1}, which is attributable to symmetric stretching of AsO_4 units. A broad band of low intensity is also observed between 450 and 525 cm^{-1}, with contributions likely originating from a range of AsO_4 vibrational modes(Plášil, 2010). An additional low-intensity mode is observed at 319 cm^{-1}, attributable specifically to ν_2 AsO_4 bending modes. Uranyl arsenate minerals included in the average spectra calculation almost exclusively crystallize in the autunite anion topology (Krivovichev et al., 2013), with the exception of walpurgite, which, while possessing U in square bipyramidal coordination, is also characterized by Bi as a structural component, irregularly coordinated by 4–5 O atoms (Frost et al., 2006f; Mereiter, 1982b). It is likely that the pronounced similarities between the structural units of all uranyl arsenates included in the average result in the relative simplicity of this

spectrum when compared with the other average spectra discussed which possess numerous U coordination environments and structure types that contribute to the average spectra. In addition to uranyl arsenates that crystallize in the autunite anion topology, some uranyl arsenates (and by analogy, phosphates) contain phosphuranylite-type sheet structures (Burns, 2005). Unfortunately, because of a dearth of these mineral species relative to the abundance of autunite type structures, and resultingly, spectra thereof, no Raman or IR data for uranyl arsenates of this type are currently included in CURIES and thus represent a high-priority target for data collection and future inclusion in the compendium.

Uranyl Carbonates

The average spectra for uranyl carbonate minerals contains contributions from andersonite ($Na_2Ca(UO_2)(CO_3)_3 \cdot 6H_2O$) (Frost et al., 2004b; Gurzhiy et al., 2018; Kalashnyk et al., 2018), bayleyite ($Mg_2(UO_2)(CO_3)_3 \cdot 18H_2O$) (Colmenero, 2020; Mayer and Mereiter, 1986; Škácha et al., 2014), liebigite ($Ca_2(UO_2)(CO_3)_3 \cdot 11H_2O$) (Frost et al., 2005e; Mereiter, 1982a), roubaultite ($Cu_2(UO_2)_3(CO_3)_2O_2(OH)_2 \cdot 4H_2O$) (Colmenero et al., 2020b), rutherfordine ($(UO_2)CO_3$) (Bonales et al., 2016a; Finch et al., 1999; Frost and Čejka, 2007), widenmannite ($Pb_2(OH)_2[(UO_2)(CO_3)_2]$) (Colmenero et al., 2020b; Plášil et al., 2010b; Plášil et al., 2014), and zellerite ($Ca(UO_2)(CO_3)_2 \cdot 5H_2O$) (Coleman et al., 1966; Frost et al., 2008e). The average spectrum is characterized by low-energy modes centered at 347 and 438 cm^{-1}. Deconvolution indicates that at least seven distinct vibrational modes contribute to intensity in this region. Intricacy here likely relates to numerous uranyl and carbonate modes appearing in this region (Bonales et al., 2016a; Plášil et al., 2017). Nine vibrational modes contribute to the apparent intensity in the uranyl region (700–900 cm^{-1}). The most distinct and intense of these modes are centered at 824 and 851 cm^{-1} and likely originate from symmetric uranyl stretching vibrations

(Bonales et al., 2016a). Similar to observations from uranyl arsenates included in CURIES, there is limited variability in the number of U coordination environments of uranyl carbonates. No square bipyramidal coordination units are found in uranyl carbonate minerals, with most U(VI) sites possessing U in pentagonal or hexagonal bipyramidal coordination, or a combination thereof. From this, we can infer that the numerous bands observed in the uranyl region of the average uranyl carbonate spectra are more closely related to variability in U-O_{yl} bond lengths (rather than coordination environments) resulting from variability in uranyl carbonate structure types.

Uranyl carbonates can be classified as mono-, di-, or tricarbonates, with the prefixes referring to the ratio of carbonate units relative to U centers(Burns, 2005). An additional structure type for uranyl carbonate minerals is characterized by finite clusters of uranyl polyhedra interconnected through charge balancing cations and/or H bonding as seen in ewingite ($Mg_8Ca_8(UO_2)_{24}(CO_3)_{30}O_4(OH)_{12}(H_2O)_{138}$), for example(Olds et al., 2017a). The variability amongst uranyl carbonate coordination environments and structure types is consistent with observed spectra as greater separation between uranyl modes is observed and individual uranyl peaks are visible by eye in the average spectra for uranyl carbonates, whereas the uranyl region in other average spectra are characterized by a more condensed cluster of bands in this region. Additional contributions in the uranyl region of uranyl carbonate minerals are manifested in an apparent doublet of modes at ~728 and 760 cm^{-1}, which are attributable to carbonate stretching and bending vibrations rather than modes originating from U-O vibrations (Bonales et al., 2016a). High-energy contributions are observed in the region between 1025 and 1150 cm^{-1}, which are also characteristic of CO_3 ν_1 symmetric stretching vibrations(Frost et al., 2008b; Frost

et al., 2006e; Plášil et al., 2017). Finally, a doublet of modes is observed at 1378 and 1400 cm^{-1} and is attributable to CO_3 ν_3 antisymmetric stretching(Frost and Čejka, 2009).

Uranyl Hydroxides and Oxyhydrates

Uranyl hydroxide and oxyhydrate average spectra were grouped together and calculated from billietite ($Ba(UO_2)6O_4(OH)_6 \cdot 4\text{-}8H_2O$) (Finch et al., 2006; Frost et al., 2007; Pagoaga et al., 1987; Vochten and Van Haverbeke, 1990), curite ($Pb_3(H_2O)_2[(UO_2)_4O_4(OH)_3]_2$)(Frost et al., 2007; Li and Burns, 2000a; Mereiter, 1979), fourmarierite ($Pb(UO_2)_4O_3(OH)_4 \cdot 4H_2O$) (Frost et al., 2007; Li and Burns, 2000b; Schindler et al., 2007), holfertite ($Ca_xU^{6+}_{2-x}Ti(O_{8-x}OH_{4x}) \cdot 3H_2O$) (Belakovskiy et al., 2006; Frost, 2011), richetite ($(Fe^{3+},Mg)Pb_{8.6}(UO_2)_{36}O_{36}(OH)_{24} \cdot 41H_2O$) (Burns, 1998b; Plášil, 2017), schoepite ($(UO_2)_8O_2(OH)_{12} \cdot 12H_2O$) (Colmenero et al., 2018a; Colmenero et al., 2019b; Finch et al., 1996; Finch et al., 1998; Kirkegaard et al., 2020; Kirkegaard et al., 2019; Weller et al., 2000), vandenbrandeite ($Cu(UO_2)(OH)_4$)(Botto et al., 2002; Colmenero et al., 2019d; Timón et al.), vandendriesscheite ($PbU_7O_{22} \cdot 12H_2O$) (Burns, 1997; Frondel et al., 1954; Frost et al., 2007), and wölsendorfite ($Pb_7(UO_2)_{14}O_{19}(OH)_4 \cdot 12H_2O$) (Burns, 1999; Plášil, 2020). While spectra for holfertite ($Ca_xU^{6+}_{2-x}Ti(O_{8-x}OH_{4x}) \cdot 3H_2O$) (Belakovskiy et al., 2006; Frost, 2011), and carlosbarbosaite ($(UO_2)_2Nb_2O_6(OH)_2 \cdot 2H_2O$), (Atencio et al., 2012) are included in our database, we have omitted them from the average spectrum calculation owing to additional metal species in the structure. Fitting results for the average uranyl hydroxide spectrum indicate that a dominant vibrational mode located at 775 cm^{-1} is the prominent contributor to broad intensity observed in the uranyl region. Other modes are present in the uranyl region at 754, 786, 805, 824, and 832 cm^{-1}. This sextet of modes indicates that there is significant variability in the position of the symmetric uranyl stretching vibrational mode in the spectra of uranyl hydroxides and oxyhydrates. This is not particularly surprising given the

structural variability seen in these mineral groups, as square, pentagonal, hexagonal bipyramidal uranium coordination environments along with combinations thereof are found in uranyl hydroxide minerals. Burns et al. (1997) note that there exists uranyl bond length variability among the three coordination environments of U(VI). Similarly, Bartlett and Cooney (1989) observe strong correlations between the position of the uranyl symmetric stretching vibrational mode in Raman spectra and the corresponding uranyl bond length. In short, this sextet of modes in the average spectra is very likely attributed to the variations in uranyl bond length arising from diverse structural modifications among minerals in this group. At lower energy, three prominent modes located at ~243, 330, and 460 cm^{-1} are observed, with deconvolution revealing that at least seven distinct modes contribute to intensity in this region. Typically, contributions here are related to equatorial U-O vibrational modes and, similar to uranyl symmetric stretching vibrational modes, might be expected to shift as a function of local coordination environments about each U center (Olds et al., 2017b; Plášil et al., 2020a). At higher energy, low-intensity modes are observed, with peaks located at 960, 1440, and 1500 cm^{-1}. The modes located at 1440 and 1500 are suggested as attributable to U-OH bending vibrations (Frost et al., 2007). Colmenero et al. recently examined the Raman spectra, physical properties, and crystal structure of the several uranyl hydroxide minerals (Colmenero et al., 2019a; Colmenero et al., 2018b; Colmenero et al., 2020a) including vandenbrandeite ($Cu(UO_2)(OH)_4$) and provide detailed spectral assignments resulting from density functional perturbation theory calculations (Colmenero et al., 2019d). Vibrational modes in vandenbrandeite centered at ~1500 cm^{-1} are attributed to combination bands consisting of spectral contributions of the ν_1 and ν_2 UO_2^{2+} vibrational modes (Colmenero et al., 2019d). However, intensity located at 960 cm^{-1} is attributed to δU-OH bending modes (Colmenero et al., 2019d). By analogy, vibrational modes located in

these regions (~1500 and 960 cm^{-1}, respectively) in the average spectra for uranyl oxyhydrates and hydroxides may be attributable to variability in ν_1 and ν_2 UO_2^{2+} combination bands and δU-OH bending modes respectively, of constituent spectra included in the average.

Uranyl Molybdates

Average uranyl molybdate spectra were calculated from data for calcurmolite ($(Ca,Na)_2(UO_2)_3Mo_2(O,OH)_{11}\cdot nH_2O$) (Frost et al., 2008c; Steciuk et al., 2020), iriginite ($(UO_2)Mo_2O_7\cdot 3H_2O$) (Frost et al., 2004a; Krivovichev and Burns, 2000b), and umohoite ($(UO_2)MoO_4\cdot 2H_2O$) (Krivovichev and Burns, 2000a) and are characterized by broad background intensity in the range of 250–1,000 cm^{-1}. Two modes are observed below 600 cm^{-1}, centered at 368 and 470 cm^{-1}, and can be attributed to MoO_4 vibrations (Frost et al., 2004a). At higher energy, between 600–1,000 cm^{-1}, an apparent pentad of modes is observed, with results of deconvolution indicating that at least seven modes contribute to intensity in this range. The complexity here is likely related to overlap between uranyl symmetric stretching and various Mo-O stretching vibrations in this region (Frost et al., 2004a; Frost et al., 2008c). As with our observations from uranyl sulfates, discussed later, inclusion of additional uranyl molybdate data in CURIES will likely improve our understanding of characteristic spectral features of this group of minerals.

Uranyl Phosphates

Average spectra for uranyl phosphate minerals were calculated from bassetite ($Fe^{2+}(UO_2)_2(PO_4)_2\cdot 10H_2O$) (Bo et al., 2016), dewindtite ($H_2Pb_3(UO_2)_2(PO_4)_4O_4\cdot 12H_2O$) (Frost et al., 2006a; Piret et al., 1990), metaautunite ($Ca(UO_2)_2(PO_4)_2\cdot 6H_2O$) (Frost and Weier, 2004a; Locock and Burns, 2003), metatorbernite ($Cu(UO_2)_2(PO_4)_2\cdot 8H_2O$) (Frost and Weier, 2004a;

Locock and Burns, 2003), metauranocircite ($Ba(UO_2)_2(PO_4)_2 \cdot 7H_2O$) (Frost, 2004; Khosrawan-Sazedj, 1982), parsonsite ($Pb_2(UO_2)(PO_4)_2$) (Burns, 2000; Frost et al., 2006b), phosphuranylite ($KCa(H_3O)_3(UO_2)_7(PO_4)_4O_4 \cdot 8H_2O$) (Demartin et al., 1991; Frost et al., 2008a), phurcalite ($Ca_2(UO_2)_3(PO_4)_2O_2 \cdot 7H_2O$) (Frost et al., 2006g; Plášil et al., 2020b), sabugalite ($HAl(UO_2)_4(PO_4)_4 \cdot 16H_2O$) (Frondel, 1951; Frost et al., 2005f), saléeite ($Mg(UO_2)_2(PO_4)_2 \cdot 10H_2O$) (Frost and Weier, 2004b; Miller and Taylor, 1986), ulrichite ($CaCu(UO_2)(PO_4)_2 \cdot 4H_2O$),(Faulques et al., 2015a; Kolitsch and Giester, 2001) and yingjiangite ($K_2Ca(UO_2)_7(PO_4)_4(OH)_6 \cdot 6H_2O$) (Frost et al., 2008a; Yuzhu and Xiaofa, 1990). Similar to observations from the average spectra of uranyl arsenates, average uranyl phosphate spectra are relatively simple and again result from structural similarities between minerals included in calculation of the average. However, there is more diversity of structure types included in the average uranyl phosphate spectra, with several constituents possessing the phosphuranylite anion topology (Burns, 2005) in addition to those having the autunite topology. These two distinct structure types might result in the observed low-energy shoulder seen at 811 cm^{-1} associated with the more prominent uranyl mode centered at 832 cm^{-1}, as variability in the position of the uranyl symmetric stretching vibrational mode is observed in the constituent spectra that contribute to this average. Several modes contribute to broad observed intensity in the range of 950–1050 cm^{-1}, which is attributable to PO_4 symmetric and/or antisymmetric stretching vibrations and might similarly be attributed to the multiple structure types included in the average spectra for uranyl phosphate minerals (Frost, 2004; Frost et al., 2008a). Low-intensity modes are observed at 274, 400, 430, 905, 1105, and 1370 cm^{-1}. The low-energy, low-intensity modes in the range of 274–430 cm^{-1} are likely related to U-O equatorial vibrations. At 605 cm^{-1}, observed intensity in the average spectra likely originates from PO_4 bending, as this mode is observed in this region of

several uranyl phosphate minerals (Frost et al., 2008a; Frost et al., 2006b). The higher energy modes at 1105, and 1370 cm^{-1} could result from arsenate and carbonate spectral contributions resulting from close mineral associations (and solid-solution in the case of arsenate impurities (Kulaszewska et al., 2019)) in sample spectra included in the average.

Uranyl Selenites

The average spectra of uranyl selenites were calculated based on the spectra of demesmaekerite ($Pb_2Cu_5(UO_2)_2(SeO_3)_6(OH)_6 \cdot 2H_2O$) (Frost et al., 2009b; Ginderow and Cesbron, 1983a), derriksite ($Cu_4(UO_2)(SeO_3)_2(OH)_6$) (Frost et al., 2014; Ginderow and Cesbron, 1983b), guilleminite ($Ba(UO_2)_3(SeO_3)_2O_2 \cdot 3H_2O$) (Cooper and Hawthorne, 1995; Frost et al., 2009a), haynesite ($(UO_2)_3(OH)_2(SeO_3)_2 \cdot 5H_2O$) (Deliens and Piret, 1991; Frost et al., 2006h), larisaite ($Na(H_3O)(UO_2)_3(SeO_3)O_2 \cdot 4H_2O$) (Chukanov et al., 2004), and marthozite ($Cu^{2+}(UO_2)_3(SeO_3)_2O_2 \cdot 8H_2O$) (Cooper and Hawthorne, 2001; Frost et al., 2008d). Uranyl selenite spectra display a triplet of modes centered at ~425 cm^{-1}. Results of deconvolution indicate that four bands likely contribute to the observed triplet. Selenite ν_4 modes are found between 387–418cm^{-1} and ν_2 bending vibrations between 460–461 cm^{-1}. A low-intensity mode is observed at ~610 cm^{-1}, and the most pronounced feature, an apparent quartet of modes, is seen between 700 and 900 cm^{-1}. Deconvolution shows that eight modes are likely contributing to the observed intensity of the quartet. Although band assignments for uranyl selenite vibrational spectra are sparse in the literature, Frost et al. note that SeO_3^{2-} symmetric stretching modes appear between 790–805 or 760–855 cm^{-1} and that ν_3 modes occur between 714–769 or 680–775 cm^{-1}, for selenite minerals (Frost et al., 2006h)(Frost and Keeffe, 2009), consistent with the complexity we observe in this region for uranyl selenites. In addition, a variety of uranyl coordination environments are present in the uranyl selenites. Demesmaekerite possesses U in

pentagonal bipyramidal coordination only, conversely, derriksite has square bipyramidal U coordination. Guilleminite, marthozite, and larisaite possess both pentagonal and hexagonal bipyramidal coordination for U. This diversity in U coordination might also contribute to the complexity observed in the uranyl region of the average uranyl selenite spectra.

Uranyl Silicates

Average spectra for uranyl silicates contain spectra for boltwoodite ($(K,Na)(UO_2)(SiO_3OH)\cdot 1.5H_2O$) (Burns, 1998a; Frost et al., 2006c), cuprosklodowskite ($Cu(UO_2)_2[(SiO_3OH]_2\cdot 6H_2O$) (Plášil et al., 2008), haiweeite ($Ca(UO_2)_2[Si_5O_{12}(OH)_2]\cdot 6H_2O$) (Plášil et al., 2013), kasolite ($Pb(UO_2)(SiO_4)\cdot H_2O$) (Colmenero et al., 2019c; Fejfarová et al., 2013), natroboltwoodite ($Na(UO_2)(SiO_3OH)\cdot H_2O$) (Burns, 1998a), sklodowskite ($Mg(UO_2)_2(SiO_3OH)_2\cdot 6H_2O$) (Mokeeva, 1959; Vochten et al., 1997), uranophane (α and β structural modifications, ($Ca(UO_2)_2(SiO_3OH)_2\cdot 5H_2O$)) (Cesbron et al., 1993; Colmenero et al., 2019e; Colmenero et al., 2018c; Ginderow, 1988), and weeksite ($K_2(UO_2)_2(Si_5O_{13})\cdot 4H_2O$) (Frost et al., 2006c; Frost et al., 2006d; Jackson and Burns, 2001). The average spectrum is characterized by a broad band of intensity in the uranyl region, centered at 795 cm^{-1}, with deconvolution suggesting that at least seven modes are contributing to this observed intensity. Similar to observations from uranyl oxyhydrates and hydroxides, the numerous modes revealed by deconvolution here were initially thought to relate to a variety of uranyl bond lengths found in uranyl silicate minerals. However, differences in bond strength are perhaps a more likely source of variability in this spectral region. All uranyl silicate spectra within CURIES are from mineral species that contain U in pentagonal bipyramidal coordination exclusively. Resultingly, differences in uranyl bond length and bond strength may result from differences in structure types of uranyl silicates included in the average spectrum calculated for these minerals. For

example, haiweeite, weeksite, and soddyite possess framework structures, whereas boltwoodite, cuprosklodowskite, kasolite, natroboltwoodite, sklodowskite, and uranophane have sheet-like structural units (Burns, 2005) despite all aforementioned minerals possessing U in pentagonal bipyramidal coordination. An apparent doublet of modes, centered at 950 cm^{-1}, is composed of three individual peaks based on results of peak fitting described previously, again likely related to differences in framework and sheet structures included in average uranyl silicate spectra and variations in Si connectivity. An additional mode, located at 975 cm^{-1}, may be indicative of Si-O vibrations (Colmenero et al., 2017; Frost et al., 2006c; Frost et al., 2006d). Numerous lower intensity modes are observed in the region between ~250 and 560 cm^{-1}. The eight modes identified in this region from deconvolution may be attributable to the variety of U-O equatorial bond lengths resulting from several possible second-sphere coordination geometries in uranyl silicates further modified by variability in water liberational vibrations and δ and ν_4 $(SiO_4)^{4-}$ modes (Colmenero et al., 2017; Frost et al., 2006c).

Uranyl Sulfates

The average uranyl sulfate Raman spectrum was calculated from just three minerals (Table 2): johannite ($Cu(UO_2)_2(SO_4)_2(OH)_2 \cdot 8H_2O$) (Frost et al., 2005d; Hurlbut Jr, 1950), marecottite ($Mg_3(UO_2)_8(SO_4)_4O_6(OH)_2 \cdot 28H_2O$) (Brugger et al., 2003; Burns et al., 2003), and uranopilite ($(UO_2)_6(SO_4)O_2(OH)_6 \cdot 14H_2O$) (Colmenero et al., 2020c; Frost et al., 2005b). Resultingly, the average spectra for uranyl sulfates are characterized by a strong vibrational mode centered at 838 cm^{-1} that is composed of three separate peaks of varying intensity upon deconvolution. Additional spectral features appear in the range of 940–1130 cm^{-1} as a pentad of modes of varying intensity. The ν_1 and ν_3 vibrational modes of SO_4 appear in this region,(Frost et al., 2005a) and at lower energy, several low-intensity modes are present with those in the range

of 420–450 and 625–670 belonging to the ν_2 and ν_4 vibrations, respectively (Makreski et al., 2005). Note that inclusion of additional data sets for uranyl sulfate minerals in CURIES and in the calculated average spectra for this group of minerals will ensure that this average spectrum more accurately represents spectroscopic features that are indicative of uranyl sulfate mineral species (Gurzhiy and Plášil, 2019; Plášil et al., 2010a). Although there are many recent publications regarding uranyl sulfate mineral species, most of which include published spectra, raw data for these minerals were not available. To this end, we have collected additional Raman spectra for seventeen uranyl sulfate minerals and will describe observations related to the changes in average spectra upon inclusion of additional data in future work.

Uranyl Vanadates

Uranyl vanadate minerals included in the average spectra for this group are carnotite ($K_2(UO_2)_2(VO_4)_2\cdot 3H_2O$) (Barton Jr, 1958), curienite ($Pb(UO_2)_2(VO_4)_2\cdot 5H_2O$) (Cesbron and Morin, 1968), francevillite ($Ba(UO_2)_2(VO_4)_2\cdot 5H_2O$) (Mereiter, 1986; Spano et al., 2017a), margaritasite ($(Cs,K,H_3O)_2(UO_2)_2(VO_4)_2\cdot H_2O$) (Wenrich-Verbeek et al., 1982), sengierite ($Cu_2(UO_2)_2(VO_4)_2\cdot 6H_2O$) (Piret et al., 1980), strelkinite ($Na_2(UO_2)_2(VO_4)_2\cdot 1H_2O$) (Alekseyeva et al., 1975), and tyuyamunite ($Ca(UO_2)_2(VO_4)_2\cdot 5\text{-}8H_2O$) (Chirvinsky, 1925; Frost et al., 2005c). Average spectra for uranyl vanadates are distinctive relative to other uranyl mineral groups. First, the most intense vibrational mode in the uranyl region, centered at 737 cm^{-1}, does not originate from symmetric stretching of uranyl O atoms; rather, it results from V in square pyramidal coordination (Frost et al., 2005c). The symmetric uranyl stretching vibrational mode is lower intensity and is found at 820 cm^{-1} in the average spectra for vanadates. Several intense vibrational modes are also observed in this average spectrum, with a strong peak located at 368 cm^{-1}, also related to V-O modes, in this case, V_2O_2 bending. In this region, results of spectral

505 deconvolution suggest that numerous vibrational modes might be contributing to observed
506 intensity, with at least six individual bands identified. An additional higher intensity mode is
507 found at higher energy, centered at 965 cm^{-1}, and is attributable to V-O symmetric stretching
508 (Frost et al., 2005c). The distinct spectra of uranyl vanadates might be directly correlated with
509 the lack of diversity in structure types for this group. All uranyl vanadate minerals for which
510 average spectra are included in CURIES possess identical sheet structures in the francevillite
511 anion topology (Burns, 2005). As a result, spectra across uranyl vanadates are quite consistent.

512 **Principal Component Spectra**

513 Towards extracting meaningful information from the large number of spectral data sets
514 included in CURIES, we performed PCA on normalized data as described in the Methods
515 Section. The reduction in dimensionality of spectroscopic data sets offered by this method has
516 allowed us to determine the most salient features present in Raman spectra included in CURIES.
517 Here, we analyze principal component spectra to elucidate spectral building blocks, or, features
518 in data sets organized by the magnitude of their spectral contributions (Beattie and Esmonde-
519 White, 2021). Areas of positive intensity in PC spectra (Figure 3) correspond to strong
520 contributions of signal in these regions. Likewise, negative intensities indicate that spectral
521 contributions are not likely in each region of the spectrum.

This is the peer-reviewed, final accepted version for American Mineralogist, published by the Mineralogical Society of America.
The published version is subject to change. Cite as Authors (Year) Title. American Mineralogist, in press.
DOI: https://doi.org/10.2138/am-2022-8738. http://www.minsocam.org/

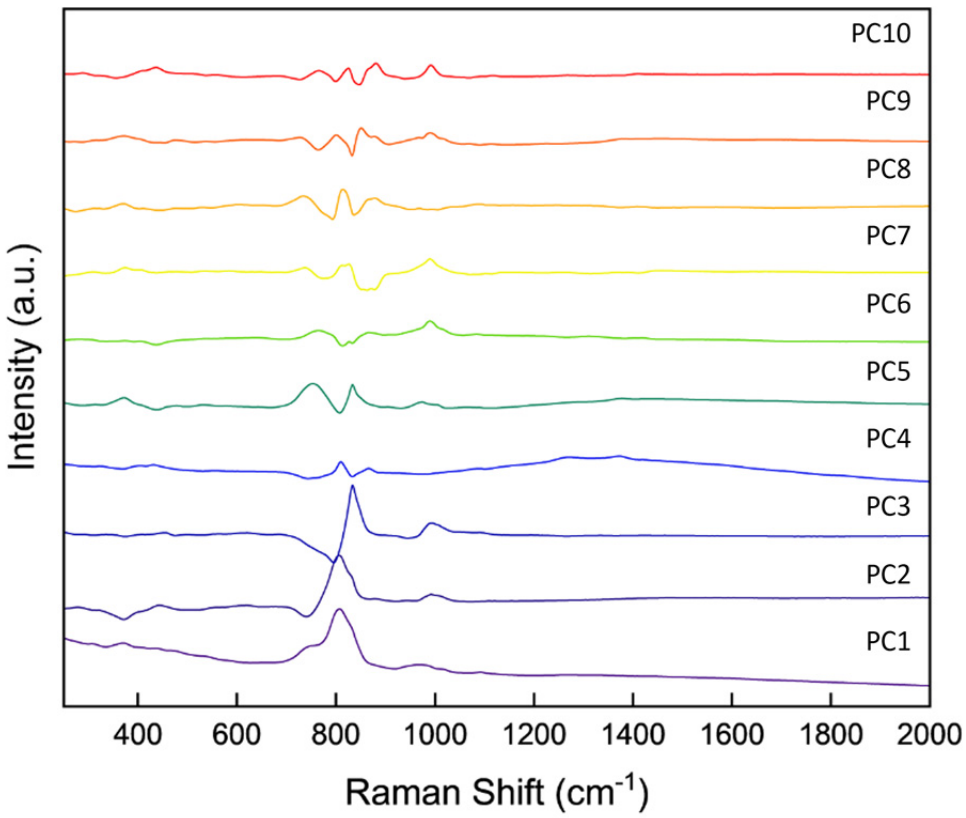

Figure 3. Principal component spectra for the first 10 principal components calculated for all 785 nm data included in CURIES. These 10 components account for 92.91% variability amongst data sets.

The first 10 principal components identified using this method are shown in Figure 3. These components account for 92.91% of total variability amongst spectra included in the analysis. Spectroscopic information in PC1 (Figure 3) accounts for 48.91% of variability amongst data sets included in this analysis and illustrates that the most prominent features in the Raman spectra of minerals included in CURIES is an intense band centered at 800 cm^{-1} and a corresponding lower energy shoulder at ~790 cm^{-1}. Less intense contributions are seen at ~375, 950, 1000, and 1050 cm^{-1}. Similarly, PC2 accounts for 13.72% of variability and is composed of an intense band centered at ~800 cm^{-1} and a lower energy contribution at 1000 cm^{-1}. PC2

contributions are also characterized by negative intensities centered at ~375 and 750 cm^{-1}. PC3, accounting for 8.69% of variability amongst spectra, is dominated by intensity centered at higher energy (~820 cm^{-1}) relative to the previous two principal components. Lower intensity contributions are observed at ~1000 cm^{-1} and a strongly negative contribution at 800 cm^{-1}. PC4 comprises 7.65 % of variability amongst spectra and is characterized by a broad band of intensity centered at ~1400 cm^{-1}, in which two intensity contributions at ~1250 and 1350 cm^{-1} are observed. Like the other components, PC4 also possesses characteristic intensity at ~810 cm^{-1} and an additional contribution at ~830 cm^{-1}. PC5 contributes 3.84% of variability amongst spectra and displays a low-intensity band centered at ~370 cm^{-1} and two bands at 750 and 830 cm^{-1}. In addition, several low-intensity modes are observed in the region between 950 and 1000 cm^{-1}. PC5 is also characterized by broad intensity above 1200 cm^{-1}, with a small band centered at 1380 cm^{-1}. PC6, accounting for 2.77% of variability amongst spectra displays negative intensity centered at 437, 809, and 835 cm^{-1} and positive intensity bands at 763, 868, and 989 cm^{-1}, with low-intensity contributions at 1084, 1311, and 1420 cm^{-1}. Band contributions in PC7, which accounts for 2.59% of spectral variability, are observed at 311, 375, 400, 740, 823, and 990 cm^{-1}, with negative intensities observed at 780 and 870 cm^{-1}. Beyond PC7, PC8, PC9, and PC10 contribute 1.94%, 1.55%, and 1.25% to total variability, respectively. Two areas of strong negative intensity are seen in PC8, located at 790 and 840 cm^{-1}, with positive contributions at 372, 395, 813, and 875 cm^{-1}. PC9 consists of low-intensity positive and negative band contributions, with positive contributions at ~375, 475, 725, 800, 850, 875, 965, and 990 cm^{-1}. Negative contributions for PC9 are located at ~770 and 830 cm^{-1}. Similar to PC9, PC10 consists of several low-intensity positive and negative spectral contributions. Positive contributions are

555 located at ~410, 438, 765, 825, 880, and 990 cm^{-1}. Low-intensity negative contributions are
556 observed at ~360, 730, 800, and 843 cm^{-1}.

557 **Oxyanion Contributions to Principal Component Spectra**

558 To extract information regarding specific contributions to principal component spectra
559 from groups of minerals based upon oxyanion chemistry, each PC spectrum shown in Figure 3
560 was compared with the average spectrum (Figure 2) for each group of uranyl minerals based on
561 oxyanion chemistry. This was done by creating overlay plots of each PC spectrum with each
562 average spectrum (Supporting Information), an example of which is shown in Figure 4. For this
563 analysis, PC1 was omitted, since the strongest contributions of this PC originate from
564 contributions in the uranyl region, the most intense region in all the average spectra. Following
565 our qualitative interpretation of spectral overlays, we also conducted partial least square
566 regression (PLSR) analysis of principal component and average spectra using a singular value
567 decomposition method to quantify the extent to which average mineral spectra contribute to each
568 principal component by determining coefficients for spectral contributions (Figure 5).
569 Correlations between principal component and average spectra for mineral groups based on
570 oxyanion chemistry are indeed observed (Figure 4) and confirm that complex interactions exist
571 between the underlying structure of uranyl minerals and their Raman spectral signatures.
572 Overlays of average and PC spectra clarify where specific structural attributes beyond the uranyl
573 mode—in particular, vibrational modes that originate from oxyanion chemistry—contribute to
574 Raman signal and can guide interpretation and identification of spectral data sets collected for
575 unknown uranium-containing materials. However, the results of PLSR shown in Figure 5 suggest
576 that more complex variability amongst spectra may be present.

This is the peer-reviewed, final accepted version for American Mineralogist, published by the Mineralogical Society of America.
The published version is subject to change. Cite as Authors (Year) Title. American Mineralogist, in press.
DOI: https://doi.org/10.2138/am-2022-8738. http://www.minsocam.org/

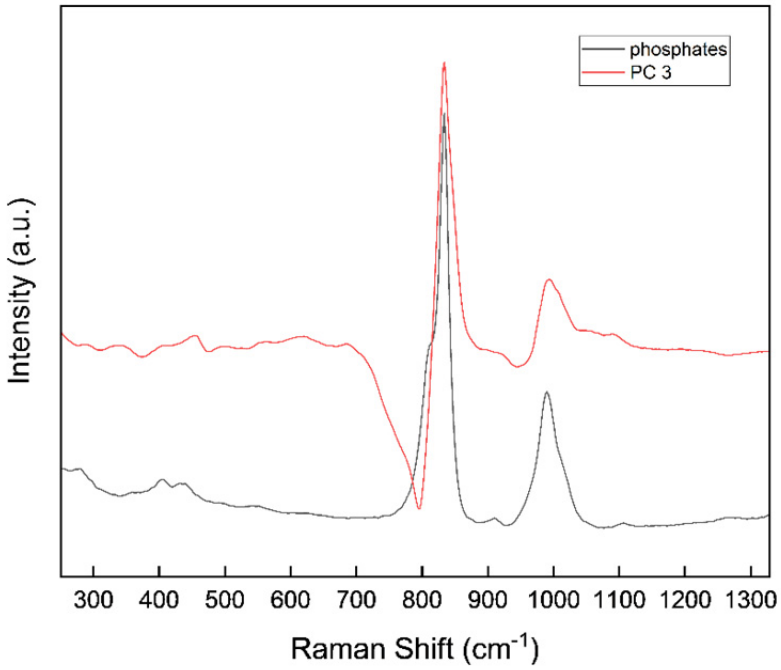

577

578 *Figure 4. Average uranyl phosphate spectra compared with the spectrum of PC3.*

579 Attributes of PC2 were found to strongly correlate with the average spectra of uranyl
580 phosphates. In particular, an area of intensity centered at ~990 cm^{-1} arising from PO_4 vibrational
581 contributions is visible in both the PC spectrum and the average phosphate spectrum. PC2 also
582 appears to possess similarities to the average spectra determined for uranyl silicates and uranyl
583 sulfates as indicated by the broadness of the 990 cm^{-1} peak, which could be partially attributable
584 to SiO and/or S-O modes observed in the average silicate and sulfate spectra. Examination of
585 Figure 5 reveals that PC2 is indeed strongly correlated with uranyl silicate, phosphate, and
586 arsenate average spectra, with a weaker correlation observed between PC2 and uranyl carbonate
587 average spectrum. PLSR results indicate that despite the apparent correlation between PC2 and
588 the average uranyl sulfate spectrum, Figure 5 shows that PC2 displays a negative correlation
589 with average uranyl sulfate, selenite, and molybdate spectra. Further, we observe that this PC is

This is the peer-reviewed, final accepted version for American Mineralogist, published by the Mineralogical Society of America.
The published version is subject to change. Cite as Authors (Year) Title. American Mineralogist, in press.
DOI: https://doi.org/10.2138/am-2022-8738. http://www.minsocam.org/

590 strongly negatively correlated with the average uranyl vanadate spectrum, suggesting there are
591 no contributions to PC2 from uranyl vanadates.

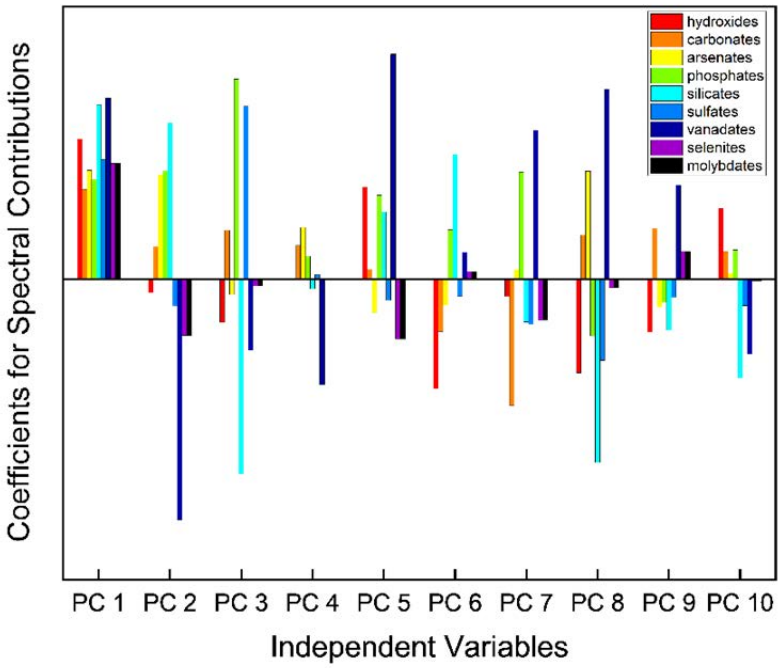

592

593 *Figure 5. Results of partial least squares regression analysis detailing mineral group spectral*
594 *contributions to principal component spectra as indicated by regression coefficients.*

595 As was observed for PC2, uranyl phosphate attributes also appear to contribute to PC3,
596 and similarly, silicate and sulfate contributions may be present as well. Figure 5 indicates that
597 quantitatively, phosphates are strongly correlated with PC3, in good agreement with visual
598 inspection of Figure 4. Additional strong contributions from sulfate average spectra are observed
599 with minor carbonate influence. In contrast to visual observations, silicate average spectra are
600 negatively correlated with PC3, as are hydroxide and vanadate average spectra. PC4 appears to
601 be strongly influenced by uranyl hydroxide spectral contributions. Broad intensity is observed
602 both in spectra for PC4 and uranyl hydroxides in the range of 1200–1600. In addition, some
603 overlap of spectral features is seen in the low-energy region between 250–400 cm^{-1}. Carbonate
604 spectra are also strongly coupled with PC4 spectra as the broad intensity is also observed in the

high-energy region of both spectra. Contributions from carbonate vibrational modes are seen in the PC4 spectra, around 1100 cm^{-1}, and lower energy contributions are visible at ~425 cm^{-1}. PC4 also shows strong similarity to average spectra for uranyl sulfates but only in the low-energy (~400 cm^{-1}) region. PLSR results suggest that the correlations predicted from overlay plots of PC4 and average uranyl sulfate spectra are misleading, as only a minor contribution from this group of minerals is observed in PC4 spectra. Strong negative correlations are observed between PC4 and uranyl vanadates, suggesting that there are very few spectral features that are similar between this PC and group of minerals.

Strong contributions to PC5 are observed from overlay plots of this principal component and average uranyl arsenate spectra in the region of AsO_4 vibrations around 900 cm^{-1}. From an overlay of uranyl phosphate average spectra, the PO_4 vibrational mode is observed in PC5 spectra, with an intense peak at ~980 cm^{-1}, and is confirmed with PLSR. Furthermore, overlapping bands are observed for uranyl phosphates and PC5 at 1375 cm^{-1}. Average uranyl silicate spectra correlate with features in the spectra for PC5 but only in the range of 425–600 cm^{-1}. The uranyl region of PC5 shows strong overlap with the uranyl region (in this case, ~830 cm^{-1}) of uranyl sulfates, and similarities between this mineral group and PC5 are also seen in the higher energy region, manifested in overlapping bands at ~975 cm^{-1}. PC5 displays some coupling to average uranyl carbonate spectra, in particular around 1050 and 1350 cm^{-1}. The strongest correlation is seen when comparing average uranyl vanadate spectra to PC5 spectra, suggesting that spectra of this mineral group dominate the spectral attributes of this PC. Strong overlap of the V-O stretching vibrations are observed in the uranyl region, and V-O bending modes, located at ~400 cm^{-1}, are also observed in PC5 spectra. Otherwise, similarities between these two spectra are seen at nearly all frequencies. The strong contributions of uranyl vanadate-

related spectral features are observed in PLSR results as well, with the highest coefficient of spectral contributions originating from the average uranyl vanadate spectrum. Although an overly of PC5 with average uranyl selenite and molybdate spectra shows some similarities, PLSR results indicate that average spectra of these two mineral groups are negatively correlated with PC5 spectral features.

From an overlay of average uranyl mineral spectra, PC6 appears to display strong similarities to uranyl phosphates. The intense feature centered at 990 cm^{-1} in the PC spectra coincides exactly with the phosphate vibrational mode, indicating strong phosphate contributions to PC6. No other strong correlations for PC6 spectra are observed from qualitative analysis of overlay plots; however, some contributions in the PC spectra might be possible at ~950 cm^{-1} arising from the Si-O mode in the average uranyl silicate spectra. This is confirmed by a strong positive correlation between PC6 and the average uranyl silicate spectrum. PLSR also indicates that minor positive correlations exist between uranyl vanadate, selenite, and molybdate spectra, whereas negative correlations exist between PC6 and uranyl hydroxide, carbonate, sulfate, and arsenate average spectra.

Overlap in the uranyl region is observed when comparing PC7 to average uranyl arsenate spectra. Similar to observations for PC6, strong correlations between the phosphate mode and PC7 are seen at ~990 cm^{-1}, and similarities thereof are confirmed by PLSR results. Qualitatively, some contributions to PC7 spectra may also arise from uranyl sulfate spectral characteristics indicated by overlap of spectral features in the range of 1000–1200 cm^{-1}; however, PLSR results suggest that there is a negative correlation between uranyl sulfate spectral features and PC7. At low energy, around 400 cm^{-1}, overlap is observed between PC7 and average uranyl vanadate spectra, suggesting that this mineral group may also contribute to PC7 spectra, which is further

651 indicated by overlap of PC7 and average vanadate spectra in the range of 990 cm^{-1} and is
652 confirmed by the high spectral contribution coefficient for vanadates and PC7. In the same low
653 energy region where overlap between average uranyl vanadate spectra is observed when
654 comparing PC7 spectra, contributions from uranyl selenites and molybdates is also possible, but
655 PLSR results indicate a negative correlation between these two mineral groups and PC7, again
656 highlighting the importance of deeper analysis beyond spectral overlays.

657 When comparing PC8 and average uranyl carbonate spectra, similarities are observed in
658 the carbonate regions (~1100 and 1300 cm^{-1}). Furthermore, uranyl modes overlap for these two
659 spectra, as similarities between PC8 and average carbonate spectra are seen at 730 cm^{-1}. Some
660 similarities between average arsenate spectra and PC8 are seen too, with coinciding peaks at
661 ~820 cm^{-1} and an overlap of uranyl peaks. PC8 also possesses similarities to uranyl vanadate
662 spectra but solely in the uranyl region and the ~400 cm^{-1} peak overlap. Carbonate, arsenate, and
663 vanadate spectral feature contributions to PC8 are confirmed by PLSR results. And, although
664 overlay plots and visual inspection of average uranyl selenites and molybdate spectra with PC8
665 show some similarities, PLSR results indicate a slight negative correlation with PC8. Negative
666 correlations for PC8 include uranyl hydroxide, arsenate, silicate, and sulfate average spectra.

667 Similarities in the OH region are observed when comparing PC9 and average uranyl
668 hydroxide spectra, although PLSR suggest a negative correlation between spectral features of
669 average uranyl hydroxide spectra and PC9. Some low-intensity contributions from average
670 uranyl carbonate spectra are observed at ~1100 cm^{-1}, 400 cm^{-1}, and 650 cm^{-1}, and carbonate
671 contributions are confirmed from PLSR. Average uranyl vanadate, selenite, and molybdate
672 spectra are also contributing to PC9 spectra in ~370, 475, and 960 cm^{-1} ranges as indicated by
673 both spectral overlays and PLSR analysis.

Overlap in the range of ~425 cm^{-1} is observed when comparing PC10 and average uranyl carbonate spectra. Lower intensity contributions may also be possible in the 1100 cm^{-1} and above range. Strong contributions are observed in PC10 from the phosphate region of the average phosphate spectra. Contributions to PC10 from uranyl hydroxide, carbonate, and phosphate average spectra are also observed from PLSR. Similarities between average sulfate and PC10 spectra may be possible based on overlay plots in particular at around 425 cm^{-1} and between 975–1150 cm^{-1}. PLSR results however, indicate negative correlations between uranyl silicate, sulfate, and vanadate spectra when compared with PC10.

Qualitative comparison of principal component and average uranyl mineral spectra based on oxyanion chemistry supported by PLSR analysis of spectral feature contributions to each PC has elucidated the influence of mineral chemistry on observed spectroscopic features and enabled several general observations. First, uranyl selenites and molybdates behave nearly identically with regard to their spectral contributions to each principal component spectra. The origins of this behavior remain unclear, but it is possible that underlying structural similarities are present between these mineral groups. Second, uranyl vanadate minerals possess unique spectra as indicated by strong negative and positive contribution coefficients to nearly all PC spectra. Third, uranyl sulfate contributions to PC spectra are generally small; and this group of minerals strongly contributes to the spectra of PC3, which may be an artifact of the small number of uranyl sulfate spectra included in CURIES. Fourth, the positive contributions of all groups of uranyl minerals to PC1 echo our observations that this component is a primary signature of U(VI) minerals encompassed by spectral features in the uranyl region. Finally, we can conclude from the results of combined PCA with PLSR that other structural features beyond oxyanion chemistry contribute to similarities between uranyl mineral spectra, as evidenced by spectral

contribution coefficients. The collection of metadata (crystal chemical information, mineral associations etc.) included in CURIES has the potential to reveal additional trends in spectroscopic contributions from uranyl minerals (and analogously, technogenic phases) beyond the influences of oxyanion chemistry explored in this work.

CURIES Status and Ongoing Work

Currently, 275 mineral species and technogenic phases are entered in CURIES, and of these, 83 phases have spectra included in the database. Through collaboration with university and museum partners, we are continuously collecting new experimental data to include in CURIES and hope that readers of this work will contribute available data by contacting the corresponding author. Synthesis of phases for which mineral specimens are unavailable is ongoing. Prioritization of phases for collection of new data has been done according to mineral groups that have the lowest ratio of included spectra to known phases (Table 2). The most complete group of uranyl minerals included in CURIES is the uranyl vanadates. Spectra are included in the database for 64% of mineral species belonging to this group. Conversely, uranyl sulfates and arsenates are the least complete, with only 10% and 18% of spectra for these mineral groups included in CURIES, respectively. Analysis of completion for groups of uranyl minerals enabled prioritization of data collection; for example, higher priority is placed on collecting additional data for uranyl sulfates than uranyl vanadates. In addition, each entry in CURIES for which spectra are not available, or are of poor quality has been triaged for the likely ease of data collection.

Conclusions

718 CURIES is the product of an extensive survey of available vibrational spectroscopic and
719 crystallographic information for secondary uranium minerals. Although there are numerous
720 applications for a large data set such as this, we have explored the possibility of using average
721 spectra for groups of minerals combined with multivariate statistical analyses to identify areas of
722 Raman spectra that contain signatures of the underlying crystal coordination chemistry to
723 elucidate possible structural origins thereof. The genesis of our work was to employ uranyl
724 minerals as analogues for understanding spectral features of materials commonly encountered in
725 the nuclear fuel cycle because of their abundance relative to uranium oxide and oxysalt
726 technogenic phases. Analysis of average spectra based on mineral group has demonstrated that
727 additional and subtle structural information is retained in mineral spectra beyond the well-
728 established signatures that originate from variability in U-O coordination environments of the
729 uranyl unit. Qualitative and quantitative comparisons of PC spectra to average spectra based on
730 mineral group have been employed to identified trends in oxyanion controls on spectroscopic
731 observables. Although CURIES is in its infancy, only containing Raman spectroscopic data for
732 ~28% of known uranium mineral species, we successfully identify common vibrational
733 spectroscopic characteristics and extract information pertaining to underlying crystal chemical
734 controls without performing expensive theoretical calculations.

735 **Implications**

736 CURIES represents a first of its kind database that includes structural and spectroscopic
737 information for uranium minerals that provides a foundation for rapid identification and analysis
738 of materials relevant to the nuclear fuel cycle. Our work represents a step towards understanding
739 the structural and chemical origins of spectroscopic observables for fuel cycle materials and,
740 more broadly, hexavalent uranium minerals. Through our analyses, we have outlined features

that can be applied to machine learning, or other advanced analytical methods, to rapidly identify nuclear materials while simultaneously serving to elucidate additional information contained within vibrational spectra.

Acknowledgments

This work was funded by the Oak Ridge National Laboratory Directed Research & Development program. The authors sincerely thank Drs. Jennifer Neu and Luke Sadergaski for their review of this work. This manuscript was greatly improved by helpful comments and feedback from Drs. Peter C. Burns, Francisco Colmenero, and Aaron Lussier.

References

Handbook of Raman Spectra for Geology, 2022.

Alekseyeva, M., Chernikov, A., Shashkin, D., Kon'kova, Y.A., and Gavrilova, I. (1975) Strelkinite, a new uranyl vanadate. International Geology Review, 17(7), 813-816.

Amme, M., Renker, B., Schmid, B., Feth, M., Bertagnolli, H., and Döbelin, W. (2002) Raman microspectrometric identification of corrosion products formed on UO_2 nuclear fuel during leaching experiments. Journal of Nuclear Materials, 306(2-3), 202-212.

Atencio, D., Roberts, A., Cooper, M., Menezes Filho, L., Coutinho, J., Stirling, J., Venance, K., Ball, N., Moffatt, E., and Chaves, M. (2012) Carlosbarbosaite, ideally $(UO_2)_2Nb_2O_6(OH)_2\cdot 2H_2O$, a new hydrated uranyl niobate mineral with tunnels from Jaguaraçu, Minas Gerais, Brazil: description and crystal structure. Mineralogical Magazine, 76(1), 75-90.

Baldridge, A.M., Hook, S.J., Grove, C., and Rivera, G. (2009) The ASTER spectral library version 2.0. Remote Sensing of Environment, 113(4), 711-715.

Bartlett, J.R., and Cooney, R.P. (1989) On the determination of uranium-oxygen bond lengths in dioxouranium (VI) compounds by Raman spectroscopy. Journal of Molecular Structure, 193, 295-300.

Barton Jr, P.B. (1958) Synthesis and properties of carnotite and its alkali analogues. American Mineralogist: Journal of Earth and Planetary Materials, 43(9-10), 799-817.

Beattie, J.R., and Esmonde-White, F.W. (2021) Exploration of principal component analysis: deriving principal component analysis visually using spectra. Applied Spectroscopy, 75(4), 361-375.

Beiswenger, T.N., Gallagher, N.B., Myers, T.L., Szecsody, J.E., Tonkyn, R.G., Su, Y.-F., Sweet, L.E., Lewallen, T.A., and Johnson, T.J. (2018) Identification of uranium minerals in natural U-bearing rocks using infrared reflectance spectroscopy. Applied Spectroscopy, 72(2), 209-224.

Belakovskiy, D., Pautov, L., Sokolova, E., Hawthorne, F., and Mokhov, A. (2006) Holfertite: a new hydroxyl-hydrated uranium titanate from Starvation Canyon, Thomas Range, Utah. The Mineralogical Record, 37(4), 311-318.

Bo, F.D., Hatert, F., Baijot, M., and Philippo, S. (2015) Crystal structure of arsenuranospathite from Rabejac, Lodève, France. European Journal of Mineralogy, 27(4), 589-597.

Bo, F.D., Hatert, F., Mees, F., Philippo, S., Baijot, M., and Fontaine, F. (2016) Crystal structure of bassetite and saléeite: new insight into autunite-group minerals. European Journal of Mineralogy, 28(3), 663-675.

Bonales, L., Colmenero, F., Cobos, J., and Timón, V. (2016a) Spectroscopic Raman characterization of rutherfordine: a combined DFT and experimental study. Physical Chemistry Chemical Physics, 18(24), 16575-16584.

Bonales, L.J., Elorrieta, J.M., Lobato, Á., and Cobos, J. (2016b) Raman spectroscopy, a useful tool to study nuclear materials. Applications of Molecular Spectroscopy to Current Research in the Chemical and Biological Sciences.

Botto, I., Barone, V., and Sanchez, M. (2002) Spectroscopic and thermal contribution to the structural characterization of vandenbrandeite. Journal of materials science, 37(1), 177-183.

Brugger, J., Burns, P.C., and Meisser, N. (2003) Contribution to the mineralogy of acid drainage of Uranium minerals: Marecottite and the zippeite-group. American Mineralogist, 88(4), 676-685.

Burns, P.C. (1997) A new uranyl oxide hydrate sheet in vandendriesscheite; implications for mineral paragenesis and the corrosion of spent nuclear fuel. American Mineralogist, 82(11-12), 1176-1186.

-. (1998a) The structure of boltwoodite and implications of solid solution toward sodium boltwoodite. The Canadian Mineralogist, 36(4), 1069-1075.

-. (1998b) The structure of richetite, a rare lead uranyl oxide hydrate. The Canadian Mineralogist, 36(1), 187-199.

-. (1999) A new complex sheet of uranyl polyhedra in the structure of wölsendorfite. American Mineralogist, 84(10), 1661-1673.

-. (2000) A new uranyl phosphate chain in the structure of parsonsite. American Mineralogist, 85(5-6), 801-805.

-. (2005) U^{6+} minerals and inorganic compounds: insights into an expanded structural hierarchy of crystal structures. The Canadian Mineralogist, 43(6), 1839-1894.

Burns, P.C., Deely, K.M., and Hayden, L.A. (2003) The crystal chemistry of the zippeite group. The Canadian Mineralogist, 41(3), 687-706.

Burns, P.C., Ewing, R.C., and Hawthorne, F.C. (1997) The crystal chemistry of hexavalent uranium: polyhedron geometries, bond-valence parameters, and polymerization of polyhedra. The Canadian Mineralogist, 35, 1551-1570.

Čejka, J. (1999) Infrared Spectroscopy and Thermal Analysis of the Uranyl Minerals. In R.F. Peter C. Burns, Ed. Uranium: Mineralogy Geochemistry and the Environment, 38, p. 521-622. Mineralogical Society of America.

Cesbron, F., Ildefonse, P., and Sichere, M.-C. (1993) New mineralogical data on uranophane and β-uranophane; synthesis of uranophane. Mineralogical Magazine, 57(387), 301-308.

Cesbron, F., and Morin, N. (1968) Une nouvelle espèce minérale: la curiénite. Étude de la série francevillite- curiénite. Bulletin de Minéralogie, 91(5), 453-459.

Chirvinsky, P.N. (1925) Tyuyamunite from the Tyuya-Muyun radium mine in Fergana. Mineralogical Magazine and Journal of the Mineralogical Society, 20(108), 287-295.

Christensen, J.N., Dresel, P.E., Conrad, M.E., Maher, K., and DePaolo, D.J. (2004) Identifying the sources of subsurface contamination at the Hanford Site in Washington using high-precision uranium isotopic measurements. Environmental Science & Technology, 38(12), 3330-3337.

826 Chukanov, N., Sidorenko, G., Naumova, I., Zadov, A., and Kuz'min, V. (2006) Chistyakovaite, a
827 New Mineral $Al(UO_2)_2(AsO_4)_2(F, OH)\cdot 6.5H_2O$. Doklady Earth Sciences, 407, p. 290.
828 Springer Nature BV.
829 Chukanov, N.V. (2013) Infrared spectra of mineral species: extended library. Springer Science &
830 Business Media.
831 Chukanov, N.V., Pushcharovsky, D.Y., Pasero, M., Merlino, S., Barinova, A.V., Mockel, S.,
832 Pekov, I.V., Zadov, A.E., and Dubinchuk, V.T. (2004) Larisaite, $Na(H_3O)(UO_2)_3$
833 $(SeO_3)_2O_2\cdot 4H_2O$, a new uranyl selenite mineral from Repete mine, San Juan County,
834 Utah, USA. European Journal of Mineralogy, 16(2), 367-374.
835 Coleman, R., Ross, D., and Meyrowitz, R. (1966) Zellerite and metazellerite, new uranyl
836 carbonates. American Mineralogist, 51(11-12), 1567-1578.
837 Colmenero, F. (2020) Thermodynamic properties of the uranyl carbonate minerals roubaultite,
838 fontanite, widenmannite, grimselite, čejkaite and bayleyite. Inorganic Chemistry
839 Frontiers, 7(21), 4160-4179.
840 Colmenero, F., Bonales, L.J., Cobos, J., and Timón, V. (2017) Structural, mechanical and
841 vibrational study of uranyl silicate mineral soddyite by DFT calculations. Journal of Solid
842 State Chemistry, 253, 249-257.
843 Colmenero, F., Cobos, J., and Timón, V. (2018a) Periodic density functional theory study of the
844 structure, Raman spectrum, and mechanical properties of schoepite mineral. Inorganic
845 chemistry, 57(8), 4470-4481.
846 -. (2019a) Periodic density functional theory study of the Raman spectrum of the hydrated uranyl
847 oxyhydroxide mineral becquerelite. Theoretical Chemistry Accounts, 138(3), 1-8.
848 Colmenero, F., Fernández, A.M., Cobos, J., and Timón, V. (2019b) Periodic DFT Study of the
849 Thermodynamic Properties and Stability of Schoepite and Metaschoepite Mineral Phases.
850 ACS Earth and Space Chemistry, 3(1), 17-28.
851 Colmenero, F., Fernández, A.M., Timón, V., and Cobos, J. (2018b) Becquerelite mineral phase:
852 crystal structure and thermodynamic and mechanical stability by using periodic DFT.
853 RSC advances, 8(43), 24599-24616.
854 Colmenero, F., Plášil, J., Cobos, J., Sejkora, J., Timón, V., Čejka, J., and Bonales, L.J. (2019c)
855 Crystal structure, hydrogen bonding, mechanical properties and Raman spectrum of the
856 lead uranyl silicate monohydrate mineral kasolite. RSC advances, 9(27), 15323-15334.
857 Colmenero, F., Plášil, J., Cobos, J., Sejkora, J., Timón, V., Čejka, J., Fernández, A.M., and
858 Petříček, V. (2019d) Structural, mechanical, spectroscopic and thermodynamic
859 characterization of the copper-uranyl tetrahydroxide mineral vandenbrandeite. RSC
860 Advances, 9(69), 40708-40726.
861 Colmenero, F., Plášil, J., and Němec, I. (2020a) Uranosphaerite: Crystal structure, hydrogen
862 bonding, mechanics, infrared and Raman spectroscopy and thermodynamics. Journal of
863 Physics and Chemistry of Solids, 141, 109400.
864 Colmenero, F., Plášil, J., and Sejkora, J. (2019e) The layered uranyl silicate mineral uranophane-
865 β: crystal structure, mechanical properties, Raman spectrum and comparison with the α-
866 polymorph. Dalton Transactions, 48(44), 16722-16736.
867 -. (2020b) The crystal structures and mechanical properties of the uranyl carbonate minerals
868 roubaultite, fontanite, sharpite, widenmannite, grimselite and čejkaite. Inorganic
869 Chemistry Frontiers, 7(21), 4197-4221.

Colmenero, F., Plášil, J., Timón, V., and Čejka, J. (2020c) Full crystal structure, hydrogen bonding and spectroscopic, mechanical and thermodynamic properties of mineral uranopilite. RSC Advances, 10(53), 31947-31960.

Colmenero, F., Timón, V., Bonales, L.J., and Cobos, J. (2018c) Structural, mechanical and Raman spectroscopic characterization of the layered uranyl silicate mineral, uranophane-α, by density functional theory methods. Clay Minerals, 53(3), 377-392.

Cooper, M.A., and Hawthorne, F.C. (1995) The crystal structure of guilleminite, a hydrated Ba-U-Se sheet structure. The Canadian Mineralogist, 33(5), 1103-1109.

-. (2001) Structure topology and hydrogen bonding in marthozite, $Cu^{2+}[(UO_2)_3(SeO_3)_2O_2](H_2O)_8$, a comparison with guilleminite, $Ba[(UO_2)_3(SeO_3)_2O_2](H_2O)_3$. The Canadian Mineralogist, 39(3), 797-807.

Corcoran, L., Simonetti, A., Spano, T.L., Lewis, S.R., Dorais, C., Simonetti, S., and Burns, P.C. (2019) Multivariate Analysis Based on Geochemical, Isotopic, and Mineralogical Compositions of Uranium-Rich Samples. Minerals, 9(9), 537.

Deliens, M., and Piret, P. (1991) La haynesite, selenite hydrate d'uranyle, nouvelle espece minerale de la Mine Repete, Comte de San Juan, Utah. The Canadian Mineralogist, 29(3), 561-564.

Demartin, F., Diella, V., Donzelli, S., Gramaccioli, C.M., and Pilati, T. (1991) The importance of accurate crystal structure determination of uranium minerals. I. Phosphuranylite $KCa(H_3O)_3(UO_2)_7(PO_4)_4O_4$. $8H_2O$. Acta Crystallographica Section B: Structural Science, 47(4), 439-446.

Driscoll, R., Wolverson, D., Mitchels, J., Skelton, J., Parker, S.C., Molinari, M., Khan, I., Geeson, D., and Allen, G.C. (2014) A Raman spectroscopic study of uranyl minerals from Cornwall, UK. RSC Advances, 4(103), 59137-59149.

Faulques, E., Kalashnyk, N., Massuyeau, F., and Perry, D. (2015a) Spectroscopic markers for uranium (VI) phosphates: a vibronic study. RSC advances, 5(87), 71219-71227.

Faulques, E., Massuyeau, F., Kalashnyk, N., and Perry, D. (2015b) Application of Raman and photoluminescence spectroscopy for identification of uranium minerals in the environment. Spectroscopy Europe, 27(1), 14-17.

Fejfarová, K., Dušek, M., Plášil, J., Čejka, J., Sejkora, J., and Škoda, R. (2013) Reinvestigation of the crystal structure of kasolite, $Pb[(UO_2)(SiO_4)](H_2O)$, an important alteration product of uraninite, UO_{2+x}. Journal of Nuclear Materials, 434(1-3), 461-467.

Finch, R., Cooper, M., Hawthorne, F., and Ewing, R. (1999) Refinement of the crystal structure of rutherfordine. The Canadian Mineralogist, 37(4), 929-938.

Finch, R.J., Burns, P.C., Hawthorne, F.C., and Ewing, R.C. (2006) Refinement of the crystal structure of billietite, $Ba[(UO_2)_6O_4(OH)_6](H_2O)_8$. The Canadian Mineralogist, 44(5), 1197-1205.

Finch, R.J., Cooper, M.A., Hawthorne, F.C., and Ewing, R.C. (1996) The crystal structure of schoepite,$[(UO_2)_8O_2(OH)_{12}](H_2O)_{12}$. The Canadian Mineralogist, 34(5), 1071-1088.

Finch, R.J., Hawthorne, F.C., and Ewing, R.C. (1998) Structural relations among schoepite, metaschoepite and" dehydrated schoepite". The Canadian Mineralogist, 36(3), 831-845.

Forsyth, R., Werme, L., and Bruno, J. (1986) The corrosion of spent UO_2 fuel in synthetic groundwater. Journal of Nuclear Materials, 138(1), 1-15.

Frondel, C. (1951) Studies of uranium minerals (VIII): Sabugalite, an aluminum-autunite. American Mineralogist, 36(9-10), 671-679.

Frondel, C., Ross, V., and Berman, E. (1954) Synthesis of Uranium Minerals: Annual Report for July 1, 1953-June 30, 1954. Department of Mineralogy-Harvard University.

Frost, R., Duong, L., and Weier, M. (2004a) Raman microscopy of the molybdate minerals koechlinite, iriginite and lindgrenite. Neues Jahrbuch fur Mineralogie, Abhandlungen, 180(3), 245-260.

Frost, R., and Weier, M. (2004a) Raman microscopy of selected autunite minerals. Neues Jahrbuch fur Mineralogie, Abhandlungen, 12, 575-594.

Frost, R., Weier, M., Bostrom, T., Cejka, J., and Martens, W. (2005a) Molecular structure of the uranyl mineral zippeite-An XRD, SEM and Raman spectroscopic study. Neues Jahrbuch fur Mineralogie, Abhandlungen, 181(3), 271-279.

Frost, R.L. (2004) An infrared and Raman spectroscopic study of the uranyl micas. Spectrochimica Acta Part A: Molecular and Biomolecular Spectroscopy, 60(7), 1469-1480.

-. (2011) Raman spectroscopic study of the uranyl titanate mineral holfertite $Ca_xU_{2-x}Ti(O_{8-x}OH_{4x})\cdot 3H_2O$ and the lack of metamictization. Radiation Effects & Defects in Solids, 166(1), 24-29.

Frost, R.L., Carmody, O., Erickson, K.L., Weier, M.L., and Čejka, J.ı. (2004b) Molecular structure of the uranyl mineral andersonite—a Raman spectroscopic study. Journal of Molecular Structure, 703(1-3), 47-54.

Frost, R.L., Carmody, O., Erickson, K.L., Weier, M.L., Henry, D.O., and Čejka, J. (2005b) Molecular structure of the uranyl mineral uranopilite—a Raman spectroscopic study. Journal of Molecular Structure, 733(1-3), 203-210.

Frost, R.L., and Čejka, J. (2007) A Raman spectroscopic study of the uranyl carbonate rutherfordine. Journal of Raman Spectroscopy, 38(11), 1488-1493.

-. (2009) A Raman spectroscopic study of the uranyl mineral rutherfordine—revisited. Journal of Raman Spectroscopy, 40(9), 1096-1103.

Frost, R.L., Čejka, J., and Ayoko, G. (2008a) Raman spectroscopic study of the uranyl phosphate minerals phosphuranylite and yingjiangite. Journal of Raman Spectroscopy, 39(4), 495-502.

Frost, R.L., Čejka, J., Ayoko, G.A., and Dickfos, M.J. (2008b) Raman spectroscopic study of the uranyl carbonate mineral voglite. Journal of Raman Spectroscopy, 39(3), 374-379.

Frost, R.L., Čejka, J., and Dickfos, M.J. (2008c) Raman and infrared spectroscopic study of the molybdate-containing uranyl mineral calcurmolite. Journal of Raman Spectroscopy, 39(7), 779-785.

-. (2009a) Raman spectroscopic study of the mineral guilleminite $Ba(UO_2)_3(SeO_3)_2(OH)_4.3H_2O$. Journal of Raman Spectroscopy, 40(4), 355-359.

-. (2009b) Raman spectroscopic study of the uranyl selenite mineral demesmaekerite $Pb_2Cu_5(UO_2)_2(SeO_3)_6(OH)_6\cdot 2H_2O$. Journal of Raman Spectroscopy, 40(5), 476-480.

Frost, R.L., Čejka, J., Keeffe, E.C., and Dickfos, M.J. (2008d) Raman spectroscopic study of the uranyl selenite mineral marthozite $Cu[(UO_2)_3(SeO_3)_2O_2]\cdot 8H_2O$. Journal of Raman Spectroscopy, 39(10), 1413-1418.

Frost, R.L., Čejka, J., Scholz, R., López, A., Theiss, F.L., and Xi, Y. (2014) Vibrational spectroscopic study of the uranyl selenite mineral derriksite $Cu_4UO_2(SeO_3)_2(OH)_6\cdot H_2O$. Spectrochimica Acta Part A: Molecular and Biomolecular Spectroscopy, 117, 473-477.

Frost, R.L., Čejka, J., Weier, M., and Ayoko, G.A. (2006a) Raman spectroscopic study of the uranyl phosphate mineral dewindtite. Journal of Raman Spectroscopy, 37(12), 1362-1367.

Frost, R.L., Čejka, J., Weier, M., and Martens, W.N. (2006b) A Raman spectroscopic study of the uranyl phosphate mineral parsonsite. Journal of Raman Spectroscopy, 37(9), 879-891.

Frost, R.L., Čejka, J., and Weier, M.L. (2007) Raman spectroscopic study of the uranyl oxyhydroxide hydrates: becquerelite, billietite, curite, schoepite and vandendriesscheite. Journal of Raman Spectroscopy, 38(4), 460-466.

Frost, R.L., Čejka, J., Weier, M.L., and Martens, W. (2006c) Molecular structure of the uranyl silicates—a Raman spectroscopic study. Journal of Raman Spectroscopy, 37(4), 538-551.

-. (2006d) A Raman and infrared spectroscopic study of the uranyl silicates—Weeksite, soddyite and haiweeite: Part 2. Spectrochimica Acta Part A: Molecular and Biomolecular Spectroscopy, 63(2), 305-312.

Frost, R.L., Čejka, J., Weier, M.L., Martens, W., and Henry, D.A. (2005c) Vibrational spectroscopy of selected natural uranyl vanadates. Vibrational spectroscopy, 39(2), 131-138.

Frost, R.L., Dickfos, M.J., and Čejka, J. (2008e) Raman spectroscopic study of the uranyl carbonate mineral zellerite. Journal of Raman Spectroscopy, 39(5), 582-586.

Frost, R.L., Erickson, K.L., Čejka, J., and Reddy, B.J. (2005d) A Raman spectroscopic study of the uranyl sulphate mineral johannite. Spectrochimica Acta part A: Molecular and Biomolecular spectroscopy, 61(11-12), 2702-2707.

Frost, R.L., Erickson, K.L., Weier, M.L., Carmody, O., and Čejka, J. (2005e) Raman spectroscopic study of the uranyl tricarbonate mineral liebigite. Journal of Molecular Structure, 737(2-3), 173-181.

Frost, R.L., and Keeffe, E.C. (2009) Raman spectroscopic study of the selenite mineral: ahlfeldite, $NiSeO_3 \cdot 2H_2O$. Journal of Raman Spectroscopy, 40(5), 509-512.

Frost, R.L., and Weier, M.L. (2004b) Hot-stage Raman spectroscopic study of the thermal decomposition of saléeite. Journal of Raman Spectroscopy, 35(4), 299-307.

Frost, R.L., Weier, M.L., Čejka, J., and Ayoko, G.A. (2006e) Raman spectroscopy of uranyl rare earth carbonate kamotoite-(Y). Spectrochimica Acta Part A: Molecular and Biomolecular Spectroscopy, 65(3-4), 529-534.

Frost, R.L., Weier, M.L., Čejka, J., and Theo Kloprogge, J. (2006f) Raman spectroscopy of walpurgite. Journal of Raman Spectroscopy, 37(5), 585-590.

Frost, R.L., Weier, M.L., Martens, W., and Čejka, J. (2006g) The structure of phurcalite—A vibrational spectroscopic study. Vibrational Spectroscopy, 41(2), 205-212.

Frost, R.L., Weier, M.L., Martens, W.N., Kloprogge, J.T., and Kristóf, J. (2005f) Thermo-Raman spectroscopic study of the uranium mineral sabugalite. Journal of Raman Spectroscopy, 36(8), 797-805.

Frost, R.L., Weier, M.L., Reddy, B.J., and Čejka, J. (2006h) A Raman spectroscopic study of the uranyl selenite mineral haynesite. Journal of Raman Spectroscopy, 37(8), 816-821.

Geipel, G., Bernhard, G., Rutsch, M., Brendler, V., and Nitsche, H. (2000) Spectroscopic properties of uranium (VI) minerals studied by time-resolved laser-induced fluorescence spectroscopy (TRLFS). Radiochimica Acta, 88(9-11), 757-762.

Ginderow, D. (1988) Structure de l'uranophane alpha, Ca (UO2) 2 (SiO3OH) 2.5 H2O. Acta Crystallographica Section C: Crystal Structure Communications, 44(3), 421-424.

Ginderow, D., and Cesbron, F. (1983a) Structure de la demesmaekerite, $Pb_2Cu_5(SeO_3)_6(UO_2)_2(OH)$ 6.2 H_2O. Acta Crystallographica Section C: Crystal Structure Communications, 39(7), 824-827.

-. (1983b) Structure de la derriksite, Cu_4 $(UO_2)(SeO_3)_2(OH)_6$. Acta Crystallographica Section C: Crystal Structure Communications, 39(12), 1605-1607.

Glebov, V. (1982) Electronic structure and properties of uranyl compounds. Relation between bond length and bond strength in uranyl compounds. Koordinatsionnaya Khimiya, 8(7), 970-976.

Gross, E.B., Corey, A.S., Mitchell, R.S., and Walenta, K. (1958) Heinrichite and metaheinrichite, hydrated barium uranyl arsenate minerals. American Mineralogist: Journal of Earth and Planetary Materials, 43(11-12), 1134-1143.

Guo, X., Ushakov, S.V., Curtius, H., Bosbach, D., and Navrotsky, A. (2014) Energetics of metastudtite and implications for nuclear waste alteration. Proceedings of the National Academy of Sciences, 111(50), 17737-17742.

Gurzhiy, V.V., Krzhizhanovskaya, M.G., Izatulina, A.R., Sigmon, G.E., Krivovichev, S.V., and Burns, P.C. (2018) Structure refinement and thermal stability studies of the uranyl carbonate mineral andersonite, $Na_2Ca[(UO_2)(CO_3)_3]\cdot(5+x)H_2O$. Minerals, 8(12), 586.

Gurzhiy, V.V., and Plášil, J. (2019) Structural complexity of natural uranyl sulfates. Acta Crystallographica Section B: Structural Science, Crystal Engineering and Materials, 75(1), 39-48.

Ho, D.M.L., Jones, A.E., Goulermas, J.Y., Turner, P., Varga, Z., Fongaro, L., Fanghänel, T., and Mayer, K. (2015) Raman spectroscopy of uranium compounds and the use of multivariate analysis for visualization and classification. Forensic science international, 251, 61-68.

Hurlbut Jr, C.S. (1950) Studies of uranium minerals (IV): Johannite. American Mineralogist: Journal of Earth and Planetary Materials, 35(7-8), 531-535.

Jackson, J.M., and Burns, P.C. (2001) A re-evaluation of the structure of weeksite, a uranyl silicate framework mineral. The Canadian Mineralogist, 39(1), 187-195.

Jones, L.H. (1958) Systematics in the vibrational spectra of uranyl complexes. Spectrochimica Acta, 10(4), 395-403.

Kalashnyk, N., Perry, D.L., Massuyeau, F., and Faulques, E. (2018) Exploring optical and vibrational properties of the uranium carbonate andersonite with spectroscopy and first-principles calculations. The Journal of Physical Chemistry C, 122(13), 7410-7420.

Khosrawan-Sazedj, F. (1982) The crystal structure of meta-uranocircite II, $Ba(UO_2)_2(PO_4)2\cdot6H_2O$. Tschermaks mineralogische und petrographische Mitteilungen, 29(3), 193-204.

Kirkegaard, M.C., Ambrogio, M.W., Miskowiec, A., Shields, A.E., Niedziela, J., Spano, T.L., and Anderson, B.B. (2020) Characterizing the degradation of $[(UO_2F_2)(H_2O)]_7.4H_2O$ under humid conditions. Journal of Nuclear Materials, 529, 151889.

Kirkegaard, M.C., Spano, T.L., Ambrogio, M.W., Niedziela, J.L., Miskowiec, A., Shields, A.E., and Anderson, B.B. (2019) Formation of a uranyl hydroxide hydrate via hydration of $[(UO_2F_2)(H_2O)]_7\cdot4H_2O$. Dalton Transactions, 48(36), 13685-13698.

Kolitsch, U., and Giester, G. (2001) Revision of the crystal structure of ulrichite, $CaCu^{2+}(UO_2)(PO_4)_2\cdot4H_2O$. Mineralogical Magazine, 65(6), 717-724.

Krivovichev, S.V., and Burns, P.C. (2000a) Crystal chemistry of uranyl molybdates. I. The structure and formula of umohoite. The Canadian Mineralogist, 38(3), 717-726.

-. (2000b) The crystal chemistry of uranyl molybdates. II. The crystal structure of iriginite. The Canadian Mineralogist, 38(4), 847-851.

Krivovichev, S.V., Plášil, J., Burns, P., and Sigmon, G. (2013) Mineralogy and crystallography of uranium. Uranium: From Cradle to Grave. Mineralogical Association of Canada Short Courses, 43, 15-119.

Kulaszewska, J., Dann, S., Warwick, P., and Kirk, C. (2019) Solid solution formation in the metatorbernite–metazeunerite system ($Cu(UO_2)_2(PO_4)_{2-x}(AsO_4)_x.nH_2O$) and their stability under conditions of variable temperature. Philosophical Transactions of the Royal Society A, 377(2147), 20180242.

Laetsch, T., and Downs, R. (2006) Software for identification and refinement of cell parameters from powder diffraction data of minerals using the RRUFF Project and American Mineralogist Crystal Structure Databases. 19th General Meeting of the International Mineralogical Association, Kobe, Japan, 23, p. e28.

Lafuente B, D.R.T., Yang H, Stone N. (2015) The power of databases: the RRUFF project. Highlights in Mineralogical Crystallography, p. 1-30. De Gruyter.

Li, Y., and Burns, P.C. (2000a) Investigations of crystal-chemical variability in lead uranyl oxide hydrates. I. Curite. The Canadian Mineralogist, 38(3), 727-735.

-. (2000b) Investigations of crystal-chemical variability in lead uranyl oxide hydrates. II. Fourmarierite. The Canadian Mineralogist, 38(3), 737-749.

Li, Y., Burns, P.C., and Gault, R.A. (2000) A new rare-earth-element uranyl carbonate sheet in the structure of bijvoetite-(Y). The Canadian Mineralogist, 38(1), 153-162.

Lin, D.H.M., Manara, D., Varga, Z., Berlizov, A., Fanghänel, T., and Mayer, K. (2013) Applicability of Raman spectroscopy as a tool in nuclear forensics for analysis of uranium ore concentrates. Radiochimica Acta, 101(12), 779-784.

Locock, A.J., and Burns, P.C. (2003) Crystal structures and synthesis of the copper-dominant members of the autunite and meta-autunite groups: torbernite, zeunerite, metatorbernite and metazeunerite. The Canadian Mineralogist, 41(2), 489-502.

Lu, G., Haes, A.J., and Forbes, T.Z. (2018) Detection and identification of solids, surfaces, and solutions of uranium using vibrational spectroscopy. Coordination chemistry reviews, 374, 314-344.

Lussier, A.J., Lopez, R.A., and Burns, P.C. (2016) A revised and expanded structure hierarchy of natural and synthetic hexavalent uranium compounds. The Canadian Mineralogist, 54(1), 177-283.

Lv, J., Li, G., Guo, S., and Shi, Y. (2016) Raman scattering from phonons and electronic excitations in UO_2 with different oxygen isotopes. Journal of Raman Spectroscopy, 47(3), 345-349.

Makreski, P., Jovanovski, G., and Dimitrovska, S. (2005) Minerals from Macedonia: XIV. Identification of some sulfate minerals by vibrational (infrared and Raman) spectroscopy. Vibrational Spectroscopy, 39(2), 229-239.

Mayer, H., and Mereiter, K. (1986) Synthetic bayleyite, $Mg_2[UO_2(CO_3)_3]\cdot 18H_2O$: Thermochemistry, crystallography and crystal structure. Tschermaks mineralogische und petrographische Mitteilungen, 35(2), 133-146.

McNamara, B., Buck, E., and Hanson, B. (2002) Observation of studtite and metastudtite on spent fuel. MRS Online Proceedings Library Archive, 757.

Mereiter, K. (1979) The crystal structure of curite, $[Pb_{6.56}(H_2O,OH)_4][(UO_2)_8O_8(OH)_6]_2$. Tschermaks mineralogische und petrographische Mitteilungen, 26(4), 279-292.

-. (1982a) The crystal structure of liebigite, $Ca_2UO_2(CO_3)_3 \cdot \sim 11H_2O$. Tschermaks mineralogische und petrographische Mitteilungen, 30(4), 277-288.

-. (1982b) The crystal structure of walpurgite, $(UO_2)Bi_4O_4(AsO_4)_2 \cdot 2H_2O$. Tschermaks mineralogische und petrographische Mitteilungen, 30(2), 129-139.

-. (1986) Crystal structure refinements of two francevillites, $(Ba,Pb)[(UO_2)_2V_2O_8].5H_2O$. Neues Jahrbuch fuer Mineralogie, Monatshefte, 552-560.

Miller, S., and Taylor, J. (1986) The crystal structure of saleeite, $Mg[UO_2PO_4]_2 \cdot 10H_2O$. Zeitschrift für Kristallographie-Crystalline Materials, 177(3-4), 247-253.

Mokeeva, V. (1959) The Crystal Structure of Sklodowskite. Doklady Akad. Nauk SSSR, 124. Vernadskii Inst. of Geochemistry and Analytical Chemistry.

Olds, T.A., Plášil, J., Kampf, A.R., Simonetti, A., Sadergaski, L.R., Chen, Y.-S., and Burns, P.C. (2017a) Ewingite: Earth's most complex mineral. Geology, 45(11), 1007-1010.

Olds, T.A., Plášil, J., Kampf, A.R., Škoda, R., Burns, P.C., Čejka, J., Bourgoin, V., and Boulliard, J.-C. (2017b) Gauthierite, $KPb[(UO_2)_7O_5(OH)_7] \cdot 8H_2O$, a new uranyl-oxide hydroxy-hydrate mineral from Shinkolobwe with a novel uranyl-anion sheet-topology. European Journal of Mineralogy, 29(1), 129-141.

Pagoaga, M.K., Appleman, D.E., and Stewart, J.M. (1987) Crystal structures and crystal chemistry of the uranyl oxide hydrates becquerelite, billietite, and protasite. American Mineralogist, 72(11-12), 1230-1238.

Palacios, M.L., and Taylor, S.H. (2000) Characterization of uranium oxides using in situ micro-Raman spectroscopy. Applied Spectroscopy, 54(9), 1372-1378.

Piret, P., Declercq, J.-P., and Wauters-Stoop, D. (1980) Crystal structure of sengierite. Bull. Mineral.;(France), 103(2).

Piret, P., Piret-Meunier, J., and Deliens, M. (1990) Composition chimique et structure cristalline de la dewindtite $Pb_3[H(UO_2)_3O_2\ (PO_4)_2]_2.12H_3O$. European Journal of Mineralogy, 399-406.

Plášil, Jakub, Čejka, J., Sejkora, J., Hlousek, J., Skoda, R., Novak, M., Dusek, M., Cisarova, I., Nemec, I., and Ederova, J. (2017) Linekite, $K_2Ca_3[(UO_2)(CO_3)_3]_2.8H_2O$, a new uranyl carbonate mineral from Jachymov, Czech Republic. Journal of Geosciences, 62(3), 201-213.

Plášil, J. (2014) Oxidation-hydration weathering of uraninite: the current state-of-knowledge. Journal of Geosciences, 59(2), 99-114.

-. (2017) Crystal structure of richetite revisited: Crystallographic evidence for the presence of pentavalent uranium. American Mineralogist: Journal of Earth and Planetary Materials, 102(9), 1771-1775.

-. (2018) The crystal structure of uranyl-oxide mineral schoepite,$[(UO_2)_4O(OH)_6](H_2O)_6$, revisited. Journal of Geosciences, 63(1), 65-73.

-. (2020) Crystal structure of uranyl-oxide mineral wölsendorfite revisited. constraints, 256, 0-16.

Plášil, J., Buixaderas, E., Čejka, J., Sejkora, J., Jehlička, J., and Novák, M. (2010a) Raman spectroscopic study of the uranyl sulphate mineral zippeite: low wavenumber and U–O stretching regions. Analytical and bioanalytical chemistry, 397(7), 2703-2715.

Plášil, J., Čejka, J., Sejkora, J., Škácha, P., Goliáš, V., Jarka, P., Laufek, F., Jehlička, J., Němec, I., and Strnad, L. (2010b) Widenmannite, a rare uranyl lead carbonate: occurrence, formation and characterization. Mineralogical Magazine, 74(1), 97-110.

Plášil, J., Fejfarová, K., Čejka, J., Dušek, M., Škoda, R., and Sejkora, J. (2013) Revision of the crystal structure and chemical formula of haiweeite, $Ca(UO_2)_2(Si_5O_{12})(OH)_2 \cdot 6H_2O$. American Mineralogist, 98(4), 718-723.

Plášil, J., Kampf, A.R., Olds, T.A., Sejkora, J., Škoda, R., Burns, P.C., and Čejka, J. (2020a) The new K, Pb-bearing uranyl-oxide mineral kroupaite: Crystal-chemical implications for the structures of uranyl-oxide hydroxy-hydrates. American Mineralogist: Journal of Earth and Planetary Materials, 105(4), 561-568.

Plášil, J., Kiefer, B., Ghazisaeed, S., and Philippo, S. (2020b) Hydrogen bonding in the crystal structure of phurcalite, $Ca_2[(UO_2)_3O_2(PO_4)_2] \cdot 7H_2O$: single-crystal X-ray study and TORQUE calculations. Acta Crystallographica Section B: Structural Science, Crystal Engineering and Materials, 76(3), 502-509.

Plášil, J., Palatinus, L., Rohlíček, J., Houdková, L., Klementová, M., Goliáš, V., and Škácha, P. (2014) Crystal structure of lead uranyl carbonate mineral widenmannite: Precession electron-diffraction and synchrotron powder-diffraction study. American Mineralogist, 99(2-3), 276-282.

Plášil, J., Sejkora, J., and Goliáš, V. (2008) Cuprosklodowskite from the uranium deposit Zálesí near Javorník in the Rychlebské hory Mountains (Czech Republic). Bulletin Mineralogicko-Petrologickeho Oddeleni Narodniho Muzea v Praze, 16(2).

Plášil, J., Sejkora, J., Cejka, J., Novak, M., Vinals, J., Ondrus, P., Veselovsky, F., Skacha, P., Jehlicka, J., Golias, V., Hlousek, J. (2010) Metarauchite, $Ni(UO_2)_2(AsO_4)_2 \cdot 8H_2O$, from Jáchymov, Czech Republic, and Schneeberg, Germany: a new member of the autunite group. The Canadian Mineralogist, 48(2), 335-350.

Pointurier, F., and Marie, O. (2010) Identification of the chemical forms of uranium compounds in micrometer-size particles by means of micro-Raman spectrometry and scanning electron microscope. Spectrochimica Acta Part B: Atomic Spectroscopy, 65(9-10), 797-804.

Ralph, J., and Chau, I. (2014) mindat. org—the mineral and locality database.

Schindler, M., Hawthorne, F.C., Burns, P.C., and Maurice, P.A. (2007) Dissolution of uranyl-oxide-hydroxy-hydrate minerals. IV. Fourmarierite and synthetic $Pb_2(H_2O[(UO_2)_{10}UO_{12}(OH)_6(H_2O)_2]$. The Canadian Mineralogist, 45(4), 963-981.

Schwerdt, I.J., Brenkmann, A., Martinson, S., Albrecht, B.D., Heffernan, S., Klosterman, M.R., Kirkham, T., Tasdizen, T., and McDonald Iv, L.W. (2018) Nuclear proliferomics: A new field of study to identify signatures of nuclear materials as demonstrated on alpha-UO_3. Talanta, 186, 433-444.

Sidorenko, G., Chukanov, N., Chistyakova, N., Bebeshko, G., Zadov, A., and Naumova, I. (2007) Uramarsite $(NH_4,H_3O)_2(UO)_2(AsO_4,PO_4)_2 \cdot 6H_2O$ as a new mineral of the metetorbernite group. Doklady Akademii Nauk-Rossijskaya Akademiya Nauk, 415(6), 804-808.

Škácha, P., Plášil, J., Sejkora, J., Čejka, J., Škoda, R., and Meisser, N. (2014) Unique occurrence of bayleyite, $Mg_2[(UO_2)(CO_3)_3] \cdot 18H_2O$, from Jáchymov. Bulletin Mineralogicko-Petrologickeho Oddeleni Narodniho Muzea v Praze, 22(2).

Spano, T.L., Dzik, E.A., Sharifironizi, M., Dustin, M.K., Turner, M., and Burns, P.C. (2017a) Thermodynamic investigation of uranyl vanadate minerals: Implications for structural stability. American Mineralogist: Journal of Earth and Planetary Materials, 102(6), 1149-1153.

Spano, T.L., Niedziela, J.L., Shields, A.E., McFarlane, J., Zirakparvar, A., Brubaker, Z., Kapsimalis, R.J., and Miskowiec, A. (2020a) Structural, Spectroscopic, and Kinetic Insight into the Heating Rate Dependence of Studtite and Metastudtite Dehydration. The Journal of Physical Chemistry C, 124(49), 26699-26713.

Spano, T.L., Shields, A.E., Barth, B.S., Gruidl, J.D., Niedziela, J.L., Kapsimalis, R.J., and Miskowiec, A. (2020b) Computationally Guided Investigation of the Optical Spectra of Pure β-UO_3. Inorganic Chemistry.

Spano, T.L., Simonetti, A., Wheeler, T., Carpenter, G., Freet, D., Balboni, E., Dorais, C., and Burns, P.C. (2017b) A novel nuclear forensic tool involving deposit type normalized rare earth element signatures. Terra Nova, 29(5), 294-305.

Spek, A.L. (2009) Structure validation in chemical crystallography. Acta Crystallographica Section D: Biological Crystallography, 65(2), 148-155.

Steciuk, G., Skoda, R., Rohlicek, J., and Plasil, J. (2020) Crystal structure of the uranyl-molybdate mineral calcurmolite $Ca[(UO_2)_3(MoO_4)_2(OH)_4](H_2O)˜5.0$: insights from a precession electron-diffraction tomography study. Journal of Geosciences, 65(1), 15-25.

Stefaniak, E.A., Alsecz, A., Sajó, I.E., Worobiec, A., Máthé, Z., Török, S., and Van Grieken, R. (2008) Recognition of uranium oxides in soil particulate matter by means of μ-Raman spectrometry. Journal of Nuclear Materials, 381(3), 278-283.

Stohl, F.V., and Smith, D.K. (1981) The crystal chemistry of the uranyl silicate minerals. American Mineralogist, 66(5-6), 610-625.

Sweet, L.E., Blake, T.A., Henager, C.H., Hu, S., Johnson, T.J., Meier, D.E., Peper, S.M., and Schwantes, J.M. (2013) Investigation of the polymorphs and hydrolysis of uranium trioxide. Journal of Radioanalytical and Nuclear Chemistry, 296(1), 105-110.

Timón, V., Cejka, J., Fernández, A.M., and Petrıcek, V. Structural, mechanical, spectroscopic and thermodynamic characterization of the copper-uranyl tetrahydroxide mineral vandenbrandeite. RSC Advances, 9(69).

Vochten, R., Blaton, N., Peeters, O., van Springel, K., and van Haverbeke, L. (1997) A new method of synthesis of boltwoodite and of formation of sodium boltwoodite, uranophane, sklodowskite and kasolite from boltwoodite. The Canadian Mineralogist, 35(3), 735-741.

Vochten, R., and Van Haverbeke, L. (1990) Transformation of schoepite into the uranyl oxide hydrates: becquerelite, billietite and wölsendorfite. Mineralogy and Petrology, 43(1), 65-72.

Weller, M.T., Light, M.E., and Gelbrich, T. (2000) Structure of uranium (VI) oxide dihydrate, $UO_3{\cdot}2H_2O$; synthetic meta-schoepite $(UO_2)_4O(OH)_6{\cdot}5H_2O$. Acta Crystallographica Section B: Structural Science, 56(4), 577-583.

Wenrich-Verbeek, K.J., Modreski, P.J., Zielinski, R.A., and Seeley, J.L. (1982) Margaritasite: a new mineral of hydrothermal origin from the Peña Blanca Uranium district, Mexico. American Mineralogist, 67(11-12), 1273-1289.

Wojdyr, M. (2010) Fityk: a general-purpose peak fitting program. Journal of Applied Crystallography, 43(5-1), 1126-1128.

Yuzhu, C.Z.H., and Xiaofa, G. (1990) A new uranium mineral-yingjiangite. Acta Mineralogica Sinica, 10, 02.